The SUBARU Deep Field Project: Lyman α Emitters at a Redshift of 6.6 [*][†]

Yoshiaki Taniguchi,[1] Masaru Ajiki,[1] Tohru Nagao,[1,2] Yasuhiro Shioya,[1] Takashi Murayama,[1]
Nobunari Kashikawa,[3] Keiichi Kodaira,[4] Norio Kaifu,[3] Hiroyasu Ando,[3] Hiroshi Karoji,[5]
Masayuki Akiyama,[5] Kentaro Aoki,[5] Mamoru Doi,[6] Shinobu S. Fujita,[1] Hisanori Furusawa,[5]
Tomoki Hayashino,[7] Fumihide Iwamuro,[8] Masanori Iye,[3] Naoto Kobayashi,[6] Tadayuki Kodama,[3]
Yutaka Komiyama,[5] Yuichi Matsuda,[3,7] Satoshi Miyazaki,[5] Yoshihiko Mizumoto,[3] Tomoki Morokuma,[6]
Kentaro Motohara,[6] Kyoji Nariai,[9] Koji Ohta,[8] Youichi Ohyama,[5] Sadanori Okamura,[10,11]
Masami Ouchi,[3] Toshiyuki Sasaki,[5] Yasunori Sato,[3] Kazuhiro Sekiguchi,[5] Kazuhiro Shimasaku,[10]
Hajime Tamura,[7] Masayuki Umemura,[12] Toru Yamada,[3] Naoki Yasuda,[13] and Michitoshi Yoshida[14]

[1]*Astronomical Institute, Graduate School of Science, Tohoku University, Aramaki, Aoba, Sendai 980-8578*
[2]*INAF — Osservatorio Astrofisico di Arcetri, Largo Enrico Fermi 5, 50125 Firenze, Italy*
[3]*National Astronomical Observatory of Japan, 2-21-1 Osawa, Mitaka, Tokyo 181-8588*
[4]*The Graduate University for Advanced Studies, Shonan Village, Hayama, Kanagawa 240-0193*
[5]*Subaru Telescope, National Astronomical Observatory of Japan, 650 N. A'ohoku Place, Hilo, HI 96720, USA*
[6]*Institute of Astronomy, Graduate School of Science, The University of Tokyo, 2-21-1 Osawa, Mitaka, Tokyo 181-0015*
[7]*Research Center for Neutrino Science, Graduate School of Science, Tohoku University, Aramaki, Aoba, Sendai 980-8578*
[8]*Department of Astronomy, Graduate School of Science, Kyoto University, Kitashirakawa, Sakyo, Kyoto 606-8502*
[9]*Department of Physics, Meisei University, 2-1-1 Hodokubo, Hino, Tokyo 191-8506*
[10]*Department of Astronomy, Graduate School of Science, The University of Tokyo, Tokyo 113-0033*
[11]*Research Center for the Early Universe, Graduate School of Science, The University of Tokyo, Tokyo 113-0033*
[12]*Center for Computational Physics, University of Tsukuba, 1-1-1 Tennodai, Tsukuba, Ibaraki 305-8571*
[13]*Institute for Cosmic Ray Research, The University of Tokyo, Kashiwa, Chiba 277-8582*
[14]*Okayama Astrophysical Observatory, National Astronomical Observatory, Kamogata, Okayama 719-0232*

Abstract

We present new results of a deep optical imaging survey using a narrow band filter (*NB921*) centered at $\lambda = 9196$ Å together with B, V, R, i', and z' broadband filters in the sky area of the Subaru Deep Field, which has been promoted as one of legacy programs of the 8.2 m Subaru Telescope. We obtained a photometric sample of 58 Ly α emitter candidates at $z \approx 6.5$–6.6 among ~ 180 strong *NB921*-excess ($z' - NB921 > 1.0$) objects together with a color criterion of $i' - z' > 1.3$. We then obtained optical spectra of 20 objects in our *NB921*-excess sample, and identified at least nine Ly α emitters at $z \sim 6.5$–6.6, including the two emitters reported by Kodaira et al. (2003, PASJ, 55, L17). Since our Ly α-emitter candidates are free from strong amplification of gravitational lensing, we are able to discuss their observational properties from a statistical point of view. Based on these new results, we obtained a lower limit of the star-formation rate density of $\rho_{\rm SFR} \simeq 5.7 \times 10^{-4} h_{0.7} \, M_\odot \, {\rm yr}^{-1} \, {\rm Mpc}^{-3}$ at $z \approx 6.6$, being consistent with our previous estimate. We discuss the nature of star-formation activity in galaxies beyond $z = 6$.

Key words: cosmology: observations — early universe — galaxies: formation — galaxies: evolution — galaxies: starburst

1. Introduction

A simple method to understand the formation process of galaxies is to find a sample of very young galaxies at high redshift, and then to investigate their observational properties in detail. Theoretical models based on the hierarchical clustering scenario suggest that first-generation (i.e., Population III) objects could be born around $z \sim 30$ (~ 0.5 Gyr after the big bang), and then galactic systems with masses higher than $10^{10} \, M_\odot$ could be assembled after $z \sim 5$–10 (~ 1 Gyr

after the big bang) although their co-moving number density could be significantly smaller than that in the present day (e.g., Ostriker, Gnedin 1996). It is, thus, important to search for star-forming galaxies beyond redshift 5 to probe the cosmic star-formation history from very high redshift to the present day.

Surveys for such high-z galaxies have been made mostly by the optical color-selection technique [e.g., Steidel et al. (1996); Madau et al. (1996); see for the recent discovery of a galaxy at $z = 10$, Pelló et al. (2004a); note that the detection of Ly α emission line has been still in debate; see Weatherley et al. (2004); Pelló et al. (2004b)]. Indeed, recent wide-field, deep imaging surveys using the Advanced Camera for Surveys on board the Hubble Space Telescope surely found a sample of galaxies at $z \sim 6$ (Giavalisco et al. 2004b; Dickinson et al. 2004; Bouwens et al. 2004; Stanway et al. 2004a,

---

2004b). In addition, recent advances in deep optical imaging capability with 8–10 m class telescopes have enabled new searches for star-forming galaxies beyond redshift 5 (see for review, Taniguchi et al. 2003b; Spinrad 2005). In particular, imaging surveys using narrow-passband filters have proved to be an efficient way to find such galaxies (e.g., Hu et al. 2002, 2004; Kodaira et al. 2003; Maier et al. 2003; Rhoads et al. 2003, 2004). These surveys can probe objects with a high star-formation rate, even if they are too faint to be detected in color-selection procedures. Therefore, these two methods cooperate with each other to investigate young, star-forming galaxies at high redshift. It is also worthwhile noting that recent imaging-spectroscopic surveys with a grism are also capable of finding high-z LAEs. A recent such trial succeeded to find a LAE at $z = 6.518$ (Kurk et al. 2004). A serendipitous discovery of a LAE at $z = 6.545$ was also reported (Stern et al. 2004). For a review of discovery methods, see Taniguchi et al. (2003b).

The Subaru Telescope team officially started a large-scale deep-survey program in 2002 April; the Subaru Deep Field (SDF) project. Several pilot papers related to the SDF project have already been published (Maihara et al. 2001; Totani et al. 2001a, 2001b, 2001c; Ouchi et al. 2001, 2003, 2004a, 2004b; Shimasaku et al. 2003; Kashikawa et al. 2003). The main aim of this project is to investigate the formation and evolution of galaxies from very high redshift ($z \sim 7$) to the present day ($z \sim 0$) based on a set of very deep optical and near infrared (NIR) imaging data and follow-up spectroscopy in both the optical and NIR. In addition, other multi-wavelength observations will be added in the future. The overall design of the SDF project will be given elsewhere (Kashikawa et al. 2004).

Since the SDF data set is very deep in both the broad and narrow filter bands (see table 1), we will be able to contribute to the progress in searches for such high-z galaxies based on the above two methods. Using our SDF data taken in 2002, we have already found two Lyα emitters (LAEs) at $z = 6.578$ and $z = 6.541$ (Kodaira et al. 2003). The former object is the most distant Lyα emitter found in optical surveys, SDF J132418.3+271455; note that the second most distant known is HCM 6A at $z = 6.56$ (Hu et al. 2002). In this paper, we present a summary of our search for LAEs at $z \approx 6.6$ made during these two years. We adopt a flat universe with $\Omega_{matter} = 0.3$, $\Omega_{\Lambda} = 0.7$, and $h_{0.7} = H_0/(70\,\mathrm{km\,s}^{-1}\,\mathrm{Mpc}^{-1})$ throughout this paper. We use the AB system for optical magnitudes.

2. Observations

2.1. Optical Deep Imaging

We have carried out a very deep optical imaging survey in the SDF centered at α(J2000) = $13^\mathrm{h}24^\mathrm{m}38\overset{s}{.}9$ and δ(J2000) = $+27°29'25\overset{''}{.}9$ (Kashikawa et al. 2004). Optical imaging was made in the B, V, R, i', z', NB816, and NB921 bands on a central $34' \times 27'$ area of the SDF with Suprime-Cam, which consisted of 5×2 CCDs of $2k \times 4k$ pixels, with a pixel scale of $0\overset{''}{.}202\,\mathrm{pixel}^{-1}$ (Miyazaki et al. 2002) on the 8.2 m Subaru Telescope (Kaifu et al. 2000; Iye et al. 2004). The data were collected in several observing runs during a period between 2001 and 2003. A summary of the imaging observations is given in table 1.

Two narrow band filters were used to find LAEs at $z \approx 5.7$,

Table 1. Journal of optical imaging observations.

Band	Exposure time	$m_{AB}(\mathrm{lim})^*$
B	35700	28.45
V	20400	27.74
R	36000	27.80
i'	48060	27.43
z'	30240	26.62
NB816	36000	26.63
NB921	53940	26.54

* Limiting magnitude (AB) for a 3σ detection on a $2\overset{''}{.}0$ diameter aperture.

and $z \approx 6.6$. Other narrow band filters, NB704 and NB711, were also used in the SDF to map the SDF. Early results with the use of NB711 were reported by Ouchi et al. (2003) and Shimasaku et al. (2003), and those with the use of NB704 were by Shimasaku et al. (2004). In this paper, we present results obtained with the use of NB921 filter centered on $\lambda_c = 9196$ Å with a passband of $\Delta\lambda$(FWHM) = 132 Å, together with broad-band data. The central wavelength corresponds to a redshift of 6.56 for Lyα emission. Details of the filter system used in the SDF project are given in Kashikawa et al. (2004). The central wavelength corresponds to a redshift of 6.56 for Lyα emission. Results obtained by using our NB816 data will be reported elsewhere.

The individual CCD data were reduced and combined using both our own data-reduction software (Yagi et al. 2002) and IRAF. The combined images for individual bands were aligned and smoothed with Gaussian kernels to match their seeing sizes. The PSF FWHM of the final images is $0\overset{''}{.}98$. The exposure times and limiting magnitudes are listed in table 1. Photometric calibrations were made using the usual spectrophotometric standard stars. Source detection and photometry were performed using SExtractor (Bertin, Arnouts 1996) version 2.1.6. The NB921-band image was chosen to detect candidate objects, and we limit the object catalog to $NB921 \leq 26.54$, the 3σ limiting magnitude. For each object detected in the NB921 image, the i', z', and NB921 magnitudes were measured on a common aperture of $2\overset{''}{.}0$ diameter. In total, ~ 82000 objects were detected down to $NB921 = 26.54$.

The bandpass of the NB921 filter is completely included in that of the z' filter. Therefore, when the Lyman break ($\lambda_{rest} = 912$ Å), or nearly zero continuum flux at λ_{rest}(Lyα) = 1216 Å is redshifted to the z' window, Lyman-break galaxies could show some excess in the $z' - NB921$ color, even if they have little Lyα emission. In order to examine this possibility, in figure 1, we show the $z' - NB921$ color as a function of the redshift for a galaxy without Lyα emission; the model galaxy is generated by using GALAXEV (Bruzual, Charlot 2003) with parameters of $Z = 0.02$, $\tau = 1$ Gyr, and the age = 1 Gyr. Even for such a Lyman break galaxy without Lyα emission, the $z' - NB921$ color becomes as high as 0.9 mag at $z \sim 6.4$. Therefore, we required that the $z' - NB921$ color exceeds 1.0 mag for strong Lyα emitters at $z \simeq 6.6$; i.e.,
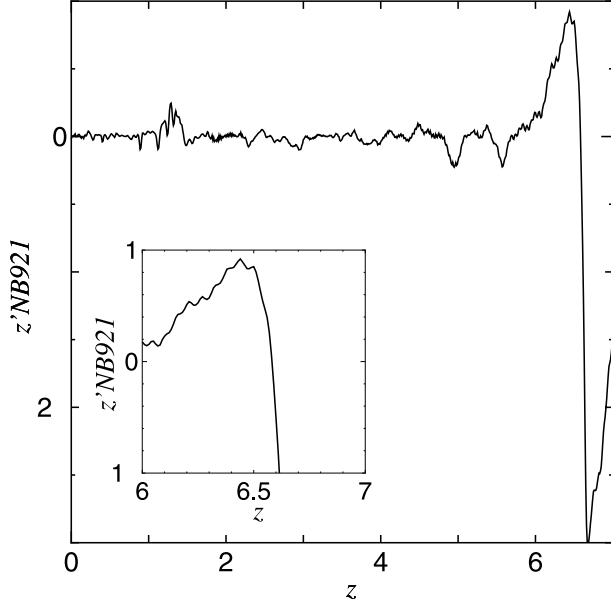
$$z' - NB921 > 1.0. \tag{1}$$

Fig. 1. The $z' - NB921$ color for a galaxy without a Ly α emission line shown as a function of the redshift. The inset shows a close up for a redshift range between $z = 6.0$ and $z = 7.0$.

Fig. 2. Color–magnitude diagram between $z' - NB921$ and $NB921$. All objects detected down to the apparent magnitude of $NB921 = 26.5$ in the $NB921$-selected catalog are shown. The horizontal red solid line corresponds to the color of $z' - NB921 = 1.0$ and the vertical red one corresponds to the 5σ limiting magnitude of $NB921 = 26.0$. The dashed curve shows the distribution of 3σ error in the color of $z' - NB921$. The 58 LAE candidates in the photometric sample are shown by filled circles, the twenty ones in the spectroscopic sample by filled circles with a large open circle, while the nine LAEs confirmed by our spectroscopy (see subsection 3.1) are shown with the same symbol but with a red large open circle. Data points without detection at z' are shown with a upper arrow; note that one σ z' magnitude is adopted.

Together with this criterion, we also used the following two more selection criteria to select $NB921$-excess objects:

$$z' - NB921 > 3\sigma \tag{2}$$

and

$$NB921 < 26.0 \ (5\sigma). \tag{3}$$

Although our 3σ detection limit for $NB921$ was 26.54, we adopted the above 5σ limit to secure the selection of $NB921$-excess objects. Using these criteria, we obtain a sample of 185 $NB921$-excess objects. In figure 2, we show a diagram between $z' - NB921$ and $NB921$, where these criteria are also shown.

In order to reduce contamination from foreground objects that are free from absorption by the intergalactic medium, we adopted another color criterion,

$$i' - z' > 1.3, \tag{4}$$

together with that LAE candidates are not detected in B, V, and R band images (less than 3σ in each band). In order to show this color criterion, we plot a diagram between $z' - NB921$ and $i' - z'$ in figure 3. We also show the color evolution of a model galaxy as a function of the redshift; colors of a starburst galaxy were calculated by using the population synthesis model GALAXEV (Bruzual, Charlot 2003) where we adopted the $\tau = 1\,\mathrm{Gyr}$ model with an age of $t = 1\,\mathrm{Gyr}$ and adding some emission lines, e.g., Ly α, [O II], and [O III]. The emission-line luminosities were calculated in the following way: (i) the Hβ luminosity was calculated from the ionizing photon production rate, N_{Lyc} photons s^{-1}, using the relation

$$L(\mathrm{H}\beta)(\mathrm{erg\ s^{-1}}) = 4.76 \times 10^{-13} N_{\mathrm{Lyc}}(\mathrm{s^{-1}}), \tag{5}$$

and (ii) the other emission-line luminosities are calculated using the relative luminosity to Hβ luminosity tabulated in PEGASE (Fioc, Rocca-Volmerange 1997).
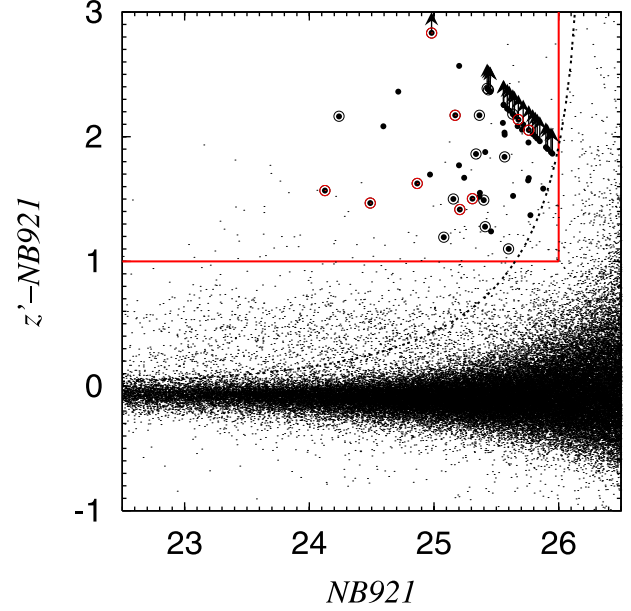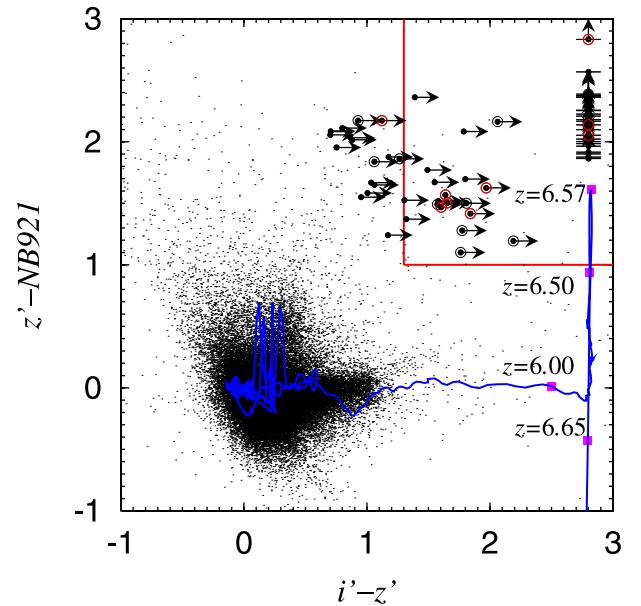

Fig. 3. Diagram between $z' - NB921$ and $i' - z'$. The meanings of the symbols are the same as those in figure 2. See the text for the color evolution of a model galaxy (blue curve).

In order not to miss possible faint LAEs, we included all objects with $z' - NB921 > 1.0$ even fainter than $i' = 27.87$ ($\simeq 2\sigma$ limiting mag) in our LAE sample. Part of them nominally had $i' - z' > 1.3$, although we did not use the $i' - z'$ color criterion for objects fainter than $z' \simeq 26.57$ ($= 27.87 - 1.3$). By using all of these criteria, we obtained a photometric sample of 58 LAE candidates. Their basic properties are given in table 2. In this table, we also give a pure z'-band magnitude, z_{9500}, for each object. This magnitude was corrected for the contribution of the Lyα flux, estimated by using the $NB921$ magnitude. The corresponding pure z'-band flux was estimated as

$$f_{9500} = [\Delta\lambda_{z'} f(z') - 0.7\Delta\lambda_{NB921} f(NB921)]/\Delta\lambda_{z'}^{\mathrm{eff}}, \qquad (6)$$

where $f(z')$ and $f(NB921)$ are the observed z' and $NB921$ fluxes, respectively, $\Delta\lambda_{z'}$ is the bandpass of the z' filter in units of Å ($= 960$ Å), $\Delta\lambda_{NB921}$ is that of the $NB921$ filter ($= 132$ Å), $\Delta\lambda_{z'}^{\mathrm{eff}}$ is the effective bandpass of the z' filter for $\lambda_{\mathrm{obs}} \geq 9260$ Å ($= 270$ Å), and the numerical factor of 0.7 is the relative transmittance of the $NB921$ filter with respect to the z' filter.

The Lyα flux corrected for the contribution of UV continuum emission at wavelengths longer than 1216 Å for each object was estimated by using

$$f_{\mathrm{Ly}\alpha,\mathrm{image}} = f(NB921) - f_\lambda(z_{9500}) \times \Delta\lambda_{NB921}/2. \qquad (7)$$

Here, we note that this sample was slightly different from that discussed in Kodaira et al. (2003) and Taniguchi (2005), because the photometric data used in their papers were based on data obtained before 2002 May and their LAE selection criteria were also different from those used in this paper. The previous LAE selection criteria adopted in Kodaira et al. (2003) were: (1) $z' - NB921 > 1.0$ and $i' - z' > 1.3$ for objects with $i' > 28.0$, and (2) $z' - NB921 > 1.0$ for objects with $i' \leq 28.0$. Note that Taniguchi (2003b) adopted $z' - NB921 > 0.9$ because the photometric sample at that occasion was tentatively selected for our follow-up optical spectroscopy. Note that the photometric catalog used in this paper is the final one described in Kashikawa et al. (2004) and thus the selection procedure of $NB921$-excess objects is also our final one.

The observed equivalent width of Lyα emission for each galaxy in our photometric sample is given in table 2. Our NB921-excess criterion given in (1) nominally corresponds to the cutoff for the Lyα-emission equivalent width, $EW_{\mathrm{obs}}(\mathrm{Ly}\alpha) > 200$ Å. However, since the actual equivalent width of Lyα emission should be obtained from $EW_{\mathrm{obs}}(\mathrm{Ly}\alpha) = f_{\mathrm{Ly}\alpha,\mathrm{image}}/f_{9500}$, the $NB921$-excess criterion given in (1) gives the equivalent width cutoff of $EW_{\mathrm{obs}}(\mathrm{Ly}\alpha) > 50$ Å, corresponding to the rest-frame equivalent width, $EW_0(\mathrm{Ly}\alpha) > 7$ Å. However, most LAE candidates in our sample tend to be faint in the z' band. Further, in order to secure the selection of LAE candidates, we also adopted the criterion (2): $z' - NB921 > 3\sigma$. Therefore, LAEs with much stronger Lyα emission could be detected in our analysis; our nine LAEs have $EW_{\mathrm{obs}}(\mathrm{Ly}\alpha) > 130$ Å (see table 2).

The effective area used to search for $NB921$-excess objects was 875.4 arcmin^2. The FWHM half-power points of the filter corresponded to a co-moving depth along the line of sight of $40.9\,h_{0.7}^{-1}$ Mpc ($z_{\mathrm{min}} \approx 6.508$ and $z_{\mathrm{max}} \approx 6.617$; note that the transmission curve of our $NB921$ filter has a Gaussian-like shape). Therefore, a total volume of $217200\,h_{0.7}^{-3}$ Mpc^3 was probed in our $NB921$ image.

2.2. Optical Spectroscopy

In order to investigate the nature of LAE candidates found in our optical-imaging survey, we obtained optical spectra of 20 objects in our photometric sample of LAEs; note that the nine galaxies for which optical spectroscopy was made were randomly selected from a photometric sample. We used the Subaru Faint Object Camera And Spectrograph (FOCAS, Kashikawa et al. 2002) on 2002 June and 2003 May and June. A journal of our spectroscopy is summarized in table 3. Details of this spectroscopy will be given elsewhere.

Our spectroscopy was made with the multi-object slit (MOS) mode using the following grating sets: (i) a 300 lines mm^{-1} grating with an O58 order cut filter, and (ii) an Echelle with a z' filter. An 0$''$8-wide slit was used in both settings. The wavelength coverage was ~ 6000 Å to 10000 Å for case (i), while it was ~ 8000 Å to 10000 Å for case (ii). The spectroscopic resolution was 9.0 Å at 9200 Å, $R \simeq 1020$, for case (i) while 6.3 Å at 9000 Å, $R \simeq 1430$, for case (ii). The spatial sampling rate was 0$''$3 pixel^{-1} after 3-pixel, on-chip binning in both cases. The flux calibration was made with spectra of spectroscopic standard stars, Hz 44 and Feige 34.

In figure 4, we show the distributions of the $NB921$ magnitudes for the photometric sample (58 objects) and the spectroscopic sample (20 objects); note that those of the spectroscopically-confirmed LAE sample (9 objects), given in subsection 3.1, are also shown. In figure 5, we show the spatial distributions of the above three samples. Details on this issue will be discussed by N. Kashikawa et al. (in preparation).

3. Results

3.1. Spectroscopic Identification

Our photometric sample of LAE candidates consisted of 58 objects. We obtained optical spectra of 20 objects among them. We detected single emission lines in 14 objects, but did not detected any emission-line feature in the remaining six objects, although one shows a marginal continuum feature.

The fourteen emission-line objects with a single emission line at $\lambda \simeq 9200$ Å may be either an LAE at $z \approx 6.6$ or an [O II] emitter at $z \approx 1.47$ (e.g., Stern et al. 2000). LAEs at high redshift show a sharp cutoff at wavelengths shortward of the line peak because of H I absorption by gas clouds in the system and intergalactic H I gas (e.g., Hu et al. 2002; Ajiki et al. 2002). Another important spectral feature of LAEs is that there is little continuum emission shortward of the Lyα line (Hu et al. 2002; Kodaira et al. 2003). Such a continuum break is actually seen in our two objects, SDF J132415.7+273058 and SDF J132418.3+271455, which are already identified as LAEs at $z \approx 6.6$ (Kodaira et al. 2003). However, the other objects show no continuum feature at wavelengths longer than the line peak, and thus we cannot identify LAEs solely by using the continuum-break feature.

Among the remaining emission-line objects, the following two have a narrow line width: 6.5 Å for SDF J132518.8+273043, and 5.5 Å for SDF J132522.3+273520.

Table 2. Photometric properties of the LAEs.[*]

No.	Name[†]	Optical AB magnitude[‡]				EW_{obs}	z
		i'	z'	NB921	z_{9500}	(Å)	
1	SDF J132352.7+271622	> 28.62	> 27.81	25.68	> 26.42	> 271	6.542
2	SDF J132353.1+271631	> 28.62	26.62	25.21	25.57	132	6.540
3	SDF J132408.3+271543	27.56	25.96	24.49	24.94	147	6.554
4	SDF J132415.7+273058[§]	27.33	25.69	24.13	24.73	181	6.541
5	SDF J132418.3+271455[§]	(28.40)	> 27.81	24.98	> 26.42	> 588	6.578
6	SDF J132418.4+273345	> 28.62	(27.34)	25.17	> 26.42	> 408	6.506
7	SDF J132432.5+271647	> 28.62	> 27.81	25.76	> 26.42	> 298	6.580
8	SDF J132518.8+273043	(28.42)	26.81	25.31	(25.81)	158	6.578
9	SDF J132522.3+273520	(28.21)	26.49	24.87	25.57	204	6.597
10	SDF J132406.5+271634	> 28.62	26.69	25.41	25.58	98	
11	SDF J132410.8+271928	> 28.62	26.27	25.08	25.13	81	
12	SDF J132417.9+271746	> 28.62	> 27.81	25.44	> 26.42	> 338	(6.55)
13	SDF J132428.7+273049	> 28.62	> 27.81	25.63	> 26.42	> 289	
14	SDF J132500.9+272030	> 28.62	(27.40)	25.57	> 26.42	> 256	
15	SDF J132515.5+273714	> 28.62	> 27.81	25.43	> 26.42	> 342	
16	SDF J132518.4+272122	> 28.62	26.40	24.24	(26.12)	732	(6.55)
17	SDF J132519.9+273704	> 28.62	(27.20)	25.34	> 26.42	> 318	(6.54)
18	SDF J132520.4+273459	> 28.62	26.89	25.40	(26.88)	154	(6.60)
19	SDF J132521.1+272712	> 28.62	26.66	25.16	25.65	157	(6.55)
20	SDF J132525.3+271932	> 28.62	26.70	25.60	25.52	65	
21	SDF J132338.4+274652	> 28.62	> 27.81	25.85	> 26.42	> 278	
22	SDF J132338.6+272940	(28.40)	26.68	25.81	> 26.42	> 258	
23	SDF J132342.2+272644	> 28.62	> 27.81	25.45	> 26.42	> 337	
24	SDF J132343.2+272452	> 28.62	26.68	24.59	(26.25)	581	
25	SDF J132347.7+272360	> 28.62	(27.66)	25.55	> 26.42	> 283	
26	SDF J132348.9+271530	> 28.62	> 27.81	25.59	> 26.42	> 309	
27	SDF J132349.2+273211	(28.50)	> 27.81	25.79	> 26.42	> 226	
28	SDF J132349.2+274546	> 28.62	27.77	25.20	> 26.42	> 429	
29	SDF J132353.4+272602	(28.10)	26.66	24.97	(25.79)	236	
30	SDF J132357.1+272448	> 28.62	(27.16)	25.63	(25.17)	165	
31	SDF J132401.5+273837	(28.53)	(27.71)	25.76	> 26.42	> 223	
32	SDF J132402.6+274653	> 28.62	26.70	25.46	25.57	90	
33	SDF J132410.5+272811	> 28.62	> 27.81	25.91	> 26.42	> 250	
34	SDF J132419.3+274125	> 28.62	> 27.81	25.56	> 26.42	> 363	
35	SDF J132422.6+274459	> 28.62	26.91	25.24	(26.02)	223	
36	SDF J132424.2+272649	(28.53)	(27.14)	25.77	(26.07)	120	
37	SDF J132425.4+272410	> 28.62	(27.58)	25.57	> 26.42	> 199	
38	SDF J132425.9+274324	> 28.62	> 27.81	25.56	> 26.42	> 271	
39	SDF J132425.0+273606	(28.56)	(27.43)	25.76	> 26.42	> 292	
40	SDF J132434.3+274056	> 28.62	> 27.81	25.71	> 26.42	> 315	
41	SDF J132435.0+273957	> 28.62	> 27.81	25.45	> 26.42	> 339	
42	SDF J132436.6+272223	> 28.62	> 27.81	25.90	> 26.42	> 229	
43	SDF J132440.2+272553	> 28.62	> 27.81	25.83	> 26.42	> 284	
44	SDF J132443.4+272633	> 28.62	26.88	25.37	(25.89)	163	
45	SDF J132444.4+273942	> 28.62	(27.29)	25.41	> 26.42	> 299	
46	SDF J132445.6+273033	(28.20)	26.97	25.20	(26.16)	276	
47	SDF J132447.7+271106	> 28.62	26.92	25.37	(25.95)	174	
48	SDF J132449.5+274237	> 28.62	(27.46)	25.88	> 26.42	> 171	
49	SDF J132450.7+272160	> 28.62	> 27.81	25.60	> 26.42	> 289	
50	SDF J132455.4+271314	> 28.62	(27.76)	25.67	> 26.42	> 252	
51	SDF J132455.8+274015	> 28.62	(27.40)	25.75	> 26.42	> 198	
52	SDF J132458.5+273913	> 28.62	(27.60)	25.56	> 26.42	> 650	
53	SDF J132458.0+272349	> 28.62	(27.08)	24.71	> 26.42	> 273	

Table 2. (Continued.)

No.	Name[†]	Optical AB magnitude[‡]				EW_{obs}	z
		i'	z'	$NB921$	z_{9500}	(Å)	
54	SDF J132503.4+273838	(28.23)	> 27.81	25.94	> 26.42	> 207	
55	SDF J132506.4+274047	> 28.62	> 27.81	25.95	> 26.42	> 193	
56	SDF J132516.7+272236	> 28.62	(27.54)	25.36	> 26.42	> 341	
57	SDF J132528.0+271328	> 28.62	(27.76)	25.71	> 26.42	> 242	
58	SDF J132533.4+271420	> 28.62	> 27.81	25.65	> 26.42	> 336	

* The LAEs are not detected in B, V, and R; see, for 3σ upper limits in these bands, table 1.
† The sky position, α(J2000) and δ(J2000), is given in the name.
‡ AB magnitude in a $2''$ diameter. The magnitudes between the 1σ and 2σ detection levels are put in parentheses.
§ LAE identified in Kodaira et al. (2003).

Table 3. Journal of optical spectroscopy.

MOS ID	Setting[*]	Exposure time	Seeing	Object IDs[†]
		(s)	($''$)	
Mask 1	300R + O58	19800	0.5–0.8	5, 7
Mask 2	300R + O58	10800	0.7–0.8	4, 6
Mask 4	Echelle + z'	14400	0.6–0.7	1, 2, 3
Mask 5	300R + O58	12600	0.6–1.0	8
Mask 6	Echelle + z'	13500	0.5–0.7	9

* Grating + order-cut filter.
† Object ID numbers that correspond to the ones given in tables 2, 4, 5, 6, and 7.
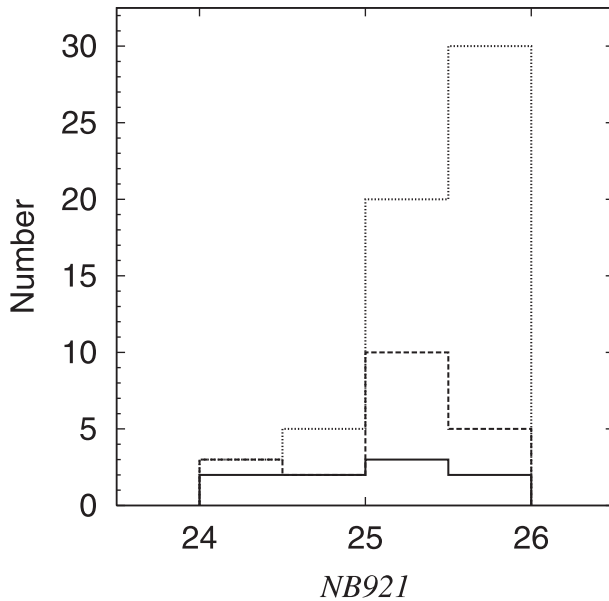
Fig. 4. Distributions of *NB921* magnitudes for the photometric sample (58 objects, dotted histograms), the spectroscopic sample (20 objects, dashed histograms), and the spectroscopically-confirmed LAE sample (9 objects, solid histograms).
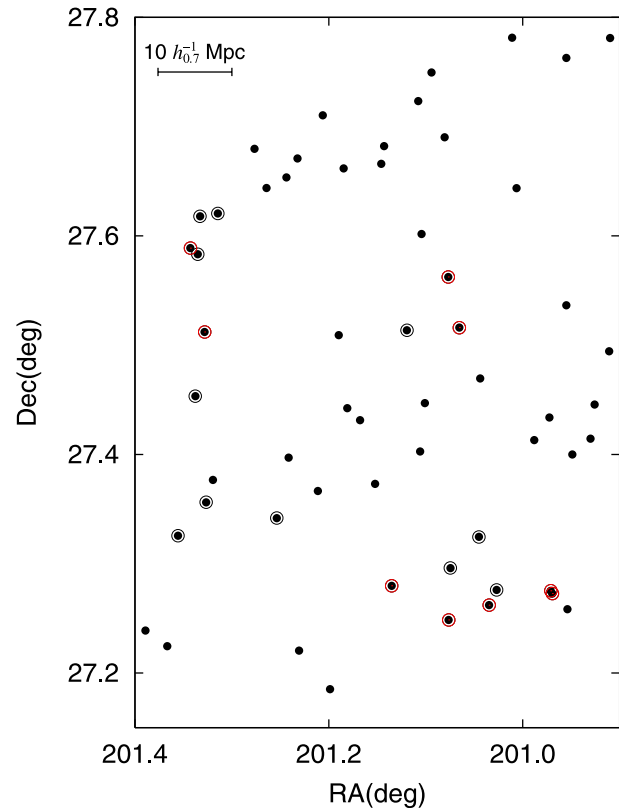

Fig. 5. Spatial distribution of the 58 objects given in our photometric sample (see table 2). The 20 LAE candidates in the spectroscopic sample are shown with a black open circle. The nine confirmed LAEs are shown with a red large open circle.

If the emission line were [O II] emission, the redshift would be $z \approx 1.47$. Since the [O II] feature is a doublet line of [O II] λ 3726.0 and [O II] λ 3728.8, the line separation would be wider than 6.9 Å at $z = 1.47$ and the two components could

be resolved in our Echelle spectroscopy. Further, if the line were Hβ, [O III] λ 4959, [O III] λ 5007, or Hα line, we would detect some other emission lines in our spectra. Therefore, these two narrow-line objects must be a LAE (e.g., Taniguchi et al. 2003a).

As for the other ten emission-line objects, we found that the following five objects show an asymmetric profile with a sharp cutoff at wavelengths shortward of the line peak: SDF J132352.7+271622, SDF J132353.1+271631, SDF J132408.3+271543, SDF J132418.4+273345, and SDF J132432.5+271647. Therefore, the nine objects discussed

Table 4. Spectral identification of emission-line objects.

ID	f_{red}/f_{blue}	$\log f_{red}/f_{blue}$
1	3.60 ± 2.08	0.556 ± 0.251
2	1.22 ± 0.43	0.086 ± 0.153
3	1.48 ± 0.32	0.170 ± 0.094
4	1.33 ± 0.41	0.124 ± 0.134
5	1.29 ± 0.40	0.111 ± 0.135
6	1.33 ± 0.18	0.124 ± 0.059
7	1.41 ± 0.46	0.149 ± 0.142
8	1.15 ± 0.54	0.061 ± 0.204
9	1.78 ± 0.43	0.250 ± 0.105
12	0.63 ± 0.47	-0.201 ± 0.324
16	0.47 ± 0.62	-0.328 ± 0.573
17	0.86 ± 0.44	-0.151 ± 0.222
18	0.86 ± 0.78	-0.151 ± 0.394
19	0.54 ± 0.57	-0.268 ± 0.459

Fig. 6. Frequency distribution of $\log f_{red}/f_{blue}$ for the sample of 9 LAEs (solid-line) and 5 single-line objects (dotted-line).

above appear to be nice candidates for LAEs at $z \approx 6.5$–6.6. The remaining five emission-line objects show either a symmetric emission-line profile or poor-S/N spectra.

In order to secure our spectral classification, we estimated the flux ratio between f_{red} and f_{blue}, where f_{red} is the flux at wavelengths longer than the emission-line peak, while f_{blue} is that at wavelengths longer than the emission-line peak. In table 4, we give our results. In figure 6, we show the frequency distribution of $\log f_{red}/f_{blue}$ for the sample of 14 emission-line objects. In this figure, we find bi-modal distributions in $\log f_{red}/f_{blue}$; i.e., the nine objects thought to be nice LAE candidates have $f_{red}/f_{blue} > 1$, while the remaining five objects have $f_{red}/f_{blue} < 1$. Some other observational tests have been proposed to identify LAEs at high redshift (e.g., Rhoads et al. 2003; Kurk et al. 2004); the S/N in our optical spectra prevents us from applying such tests.

In total, we identified nine LAEs whose emission-line shapes show a sharp cutoff at wavelengths shortward of the line peak. They are listed up in the upper part of table 2. Their optical spectra are shown in figure 7.

Since the remaining five emission-line objects show either a symmetric emission-line profile, or poor-S/N spectra, we did not include them as our final LAE sample, although we cannot rule out the possibility that they are LAEs at $z \approx 6.6$. They are listed in the middle part of table 2, with a Lyα redshift, if they are a LAE. Their spectra are shown in figure 8.

We found no emission-line feature in the six candidates in our spectroscopic sample (Nos. 10, 11, 13, 14, 15, and 20 in table 2). The estimated noises in our FOCAS spectra in these six objects range from $2 \times 10^{-19}\,\mathrm{erg\,s^{-1}\,cm^2\,\mathring{A}^{-1}}$ to $3 \times 10^{-19}\,\mathrm{erg\,s^{-1}\,cm^2\,\mathring{A}^{-1}}$. Taking account of these noises, we could detect their Lyα fluxes, expected from our *NB921* imaging, if they had an unresolved Lyα emission line in our FOCAS Echelle spectra (6.4 Å resolution), because their peak fluxes would range from $3 \times 10^{-19}\,\mathrm{erg\,s^{-1}\,cm^2\,\mathring{A}^{-1}}$ to $6 \times 10^{-19}\,\mathrm{erg\,s^{-1}\,cm^2\,\mathring{A}^{-1}}$. If the line had some broad feature, or if the line was recorded in some noisy spectral parts, it seems that it would have been quite difficult to detect unambiguous
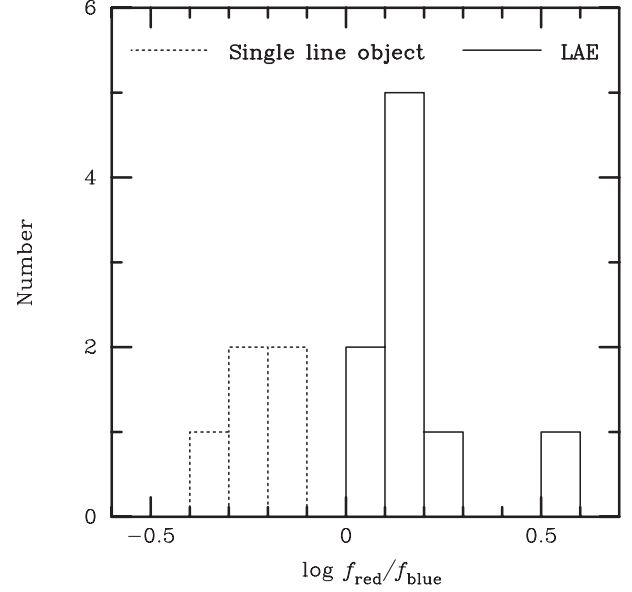
emission-line feature for these six objects in our FOCAS spectroscopy. Since there was no emission-line feature in these six objects, we cannot judge whether they are LAEs or low-z emission-line sources. Another possibility is that they might be LBGs with weak Lyα emission. In any case, we need future very deep optical spectroscopy for these objects.

Thumbnail images of the nine LAEs are shown in figure 9; their photometric properties are given in table 2. The redshift given in the last column of table 2 was estimated from the peak of the Lyα emission line. The measurement error of redshift was estimated to be ± 0.002. The observed flux of Lyα emission of each object is given in table 5. The Lyα line width is also given in this table. The line width ranges from $180\,\mathrm{km\,s^{-1}}$ to $460\,\mathrm{km\,s^{-1}}$, being comparable to those of previously identified LAEs beyond $z = 5$. Our spectra show no evidence of N V λ 1240 emission for all the nine LAEs. These properties suggest that they are star-forming galaxies, rather than active galactic nuclei. LAEs with FWHM $> 300\,\mathrm{km\,s^{-1}}$ (four among the nine) may experience a superwind in some cases (e.g., Dawson et al. 2001; Ajiki et al. 2002).

3.2. A Fraction of LAEs

Our optical spectroscopy has confirmed that 9 among 20 candidates are real LAEs at $z \approx 6.6$. Five among the remaining 11 objects are single-line emitters with a symmetric emission-line profile. They may be either a LAE at $z \sim 6.6$ or an [O II] λ 3727 emitter at $z \sim 1.47$.

Since it is safe to keep the five single-line objects as unclassified objects, we obtain from our spectroscopy that the fraction of reliable LAEs in our photometric sample is $f(\mathrm{LAE}) = 9/20 = 0.45$. This can be regarded as a lower limit in our study. If we include nominally 5 single-line emitters into the LAE sample, we obtain $f(\mathrm{LAE}) = 14/20 = 0.70$. The real fraction of LAEs in our study seems to be in the range of $f(\mathrm{LAE}) \simeq 0.45$–0.70.
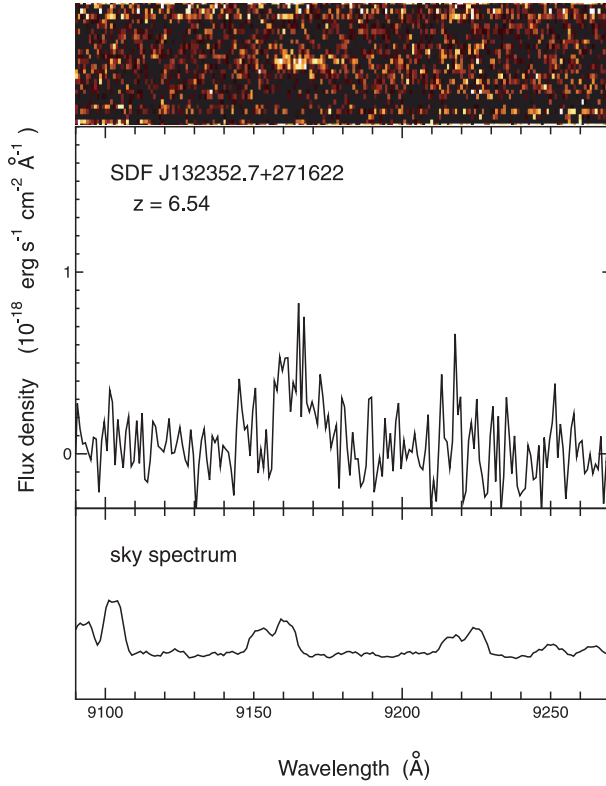
Fig. 7-1. Observed optical spectra of nine LAE candidates (No. 1 SDF J132352.7 + 271622).
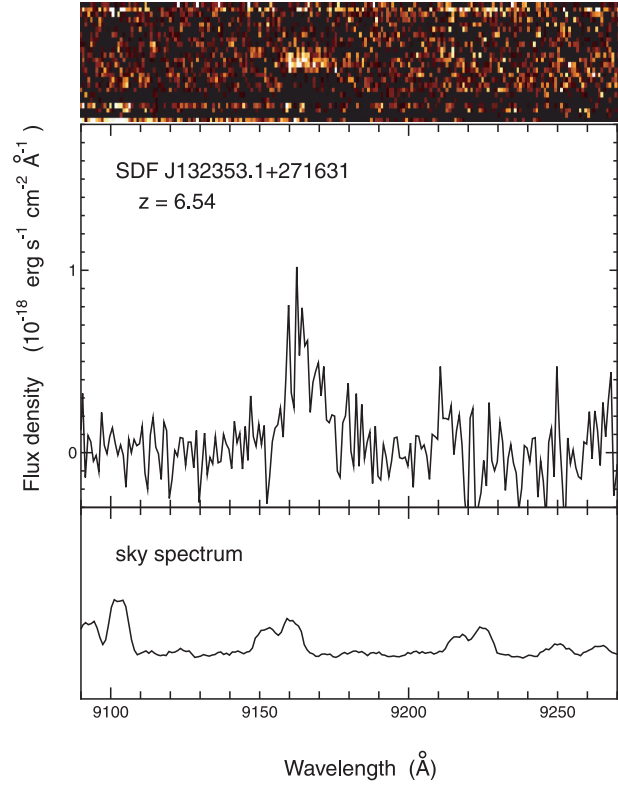

Fig. 7-2. Observed optical spectra of nine LAE candidates (No. 2 SDF J132353.1 + 271631).
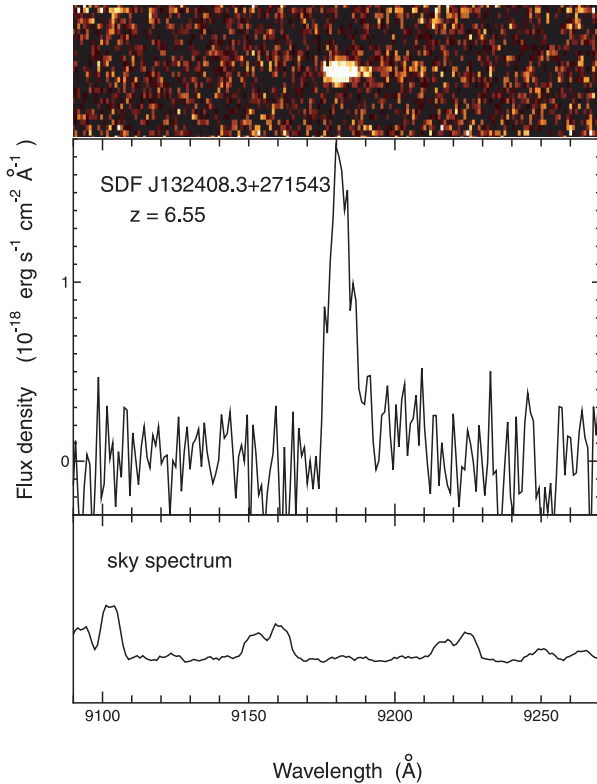

Fig. 7-3. Observed optical spectra of nine LAE candidates (No. 3 SDF J132408.3 + 271543).
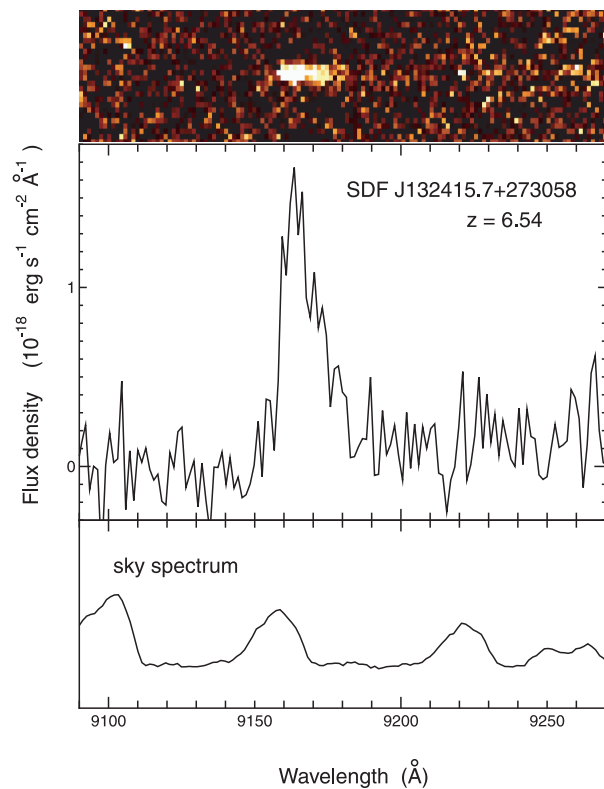

Fig. 7-4. Observed optical spectra of nine LAE candidates (No. 4 SDF J132415.7 + 273058). This object was already reported in Kodaira et al. (2003).
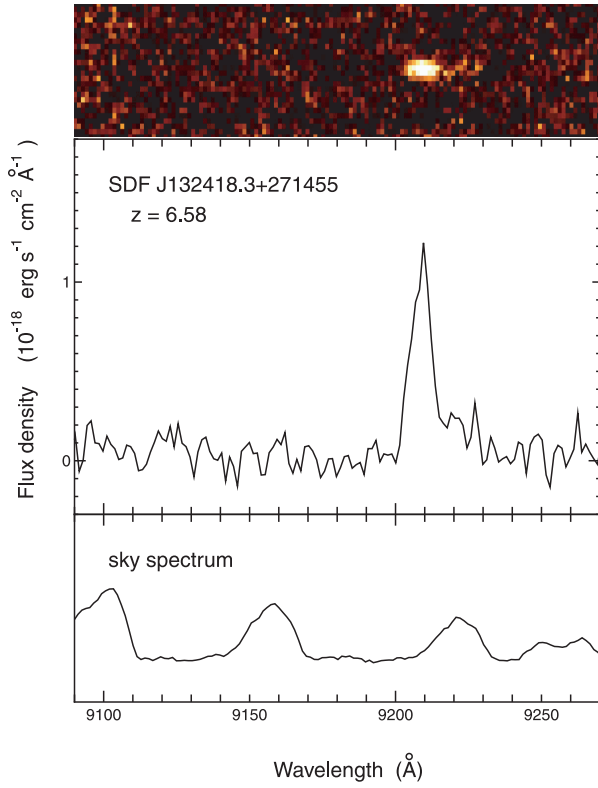
Fig. 7-5. Observed optical spectra of nine LAE candidates (No. 5 SDF J132418.3 + 271455). This object was already reported in Kodaira et al. (2003).
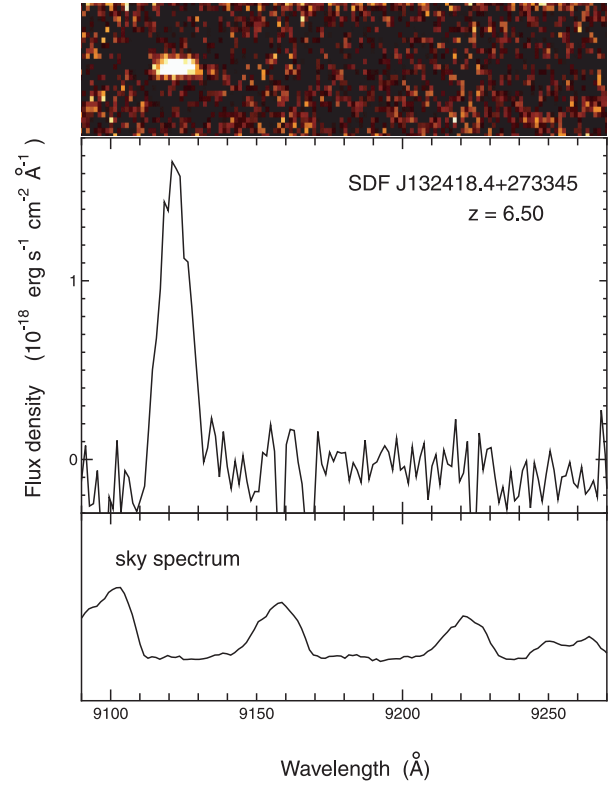
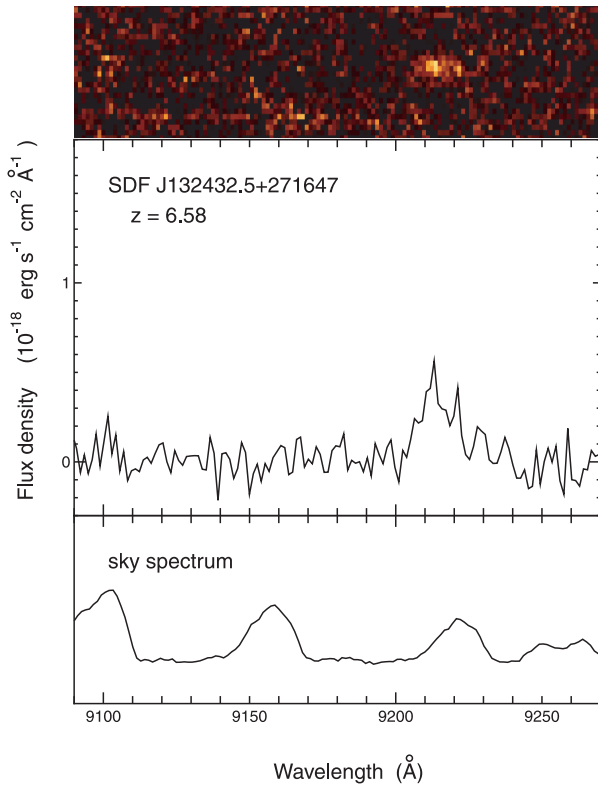**Fig. 7-6.** Observed optical spectra of nine LAE candidates (No. 6 SDF J132418.4 + 273345).

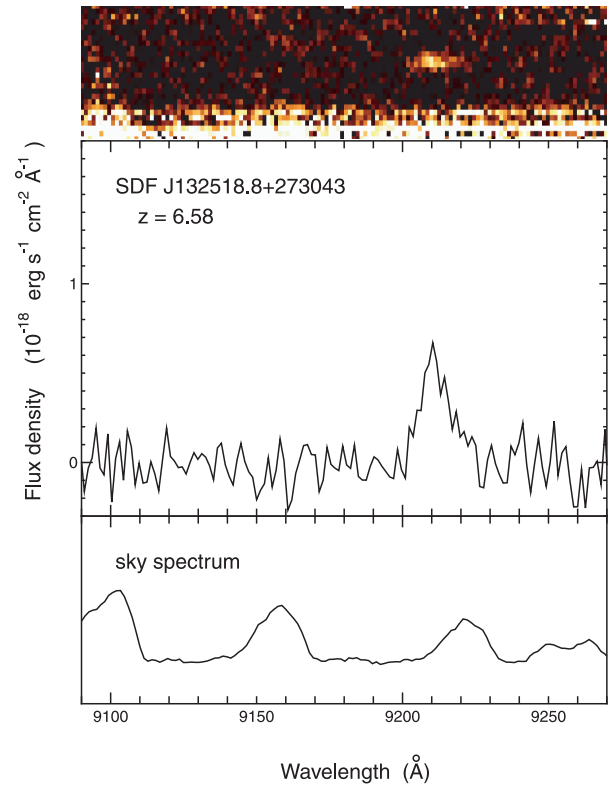**Fig. 7-7.** Observed optical spectra of nine LAE candidates (No. 7 SDF J132432.5 + 271647).

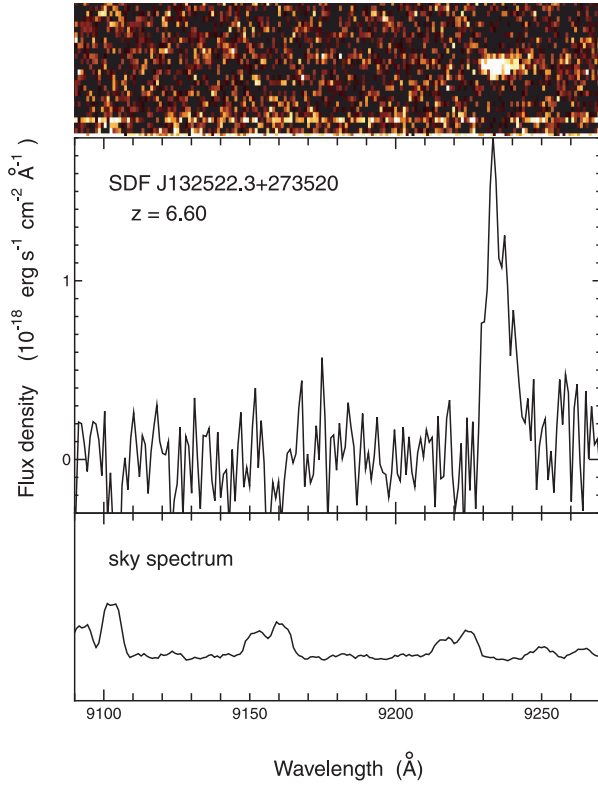**Fig. 7-8.** Observed optical spectra of nine LAE candidates (No. 8 SDF J132518.8 + 273043).

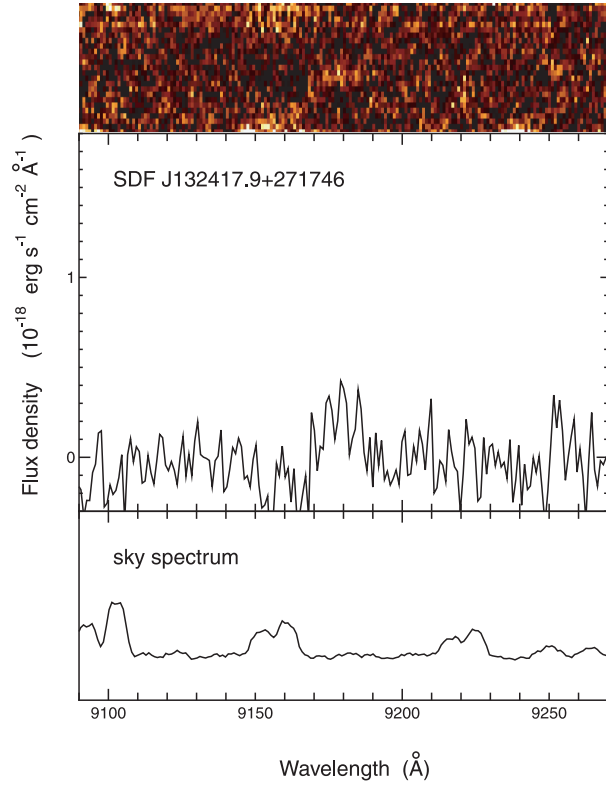**Fig. 7-9.** Observed optical spectra of nine LAE candidates (No. 9 SDF J132522.3 + 273520).

Fig. 8-1. Observed optical spectra of five single-line objects (No. 12 SDF J132417.9 + 271746).
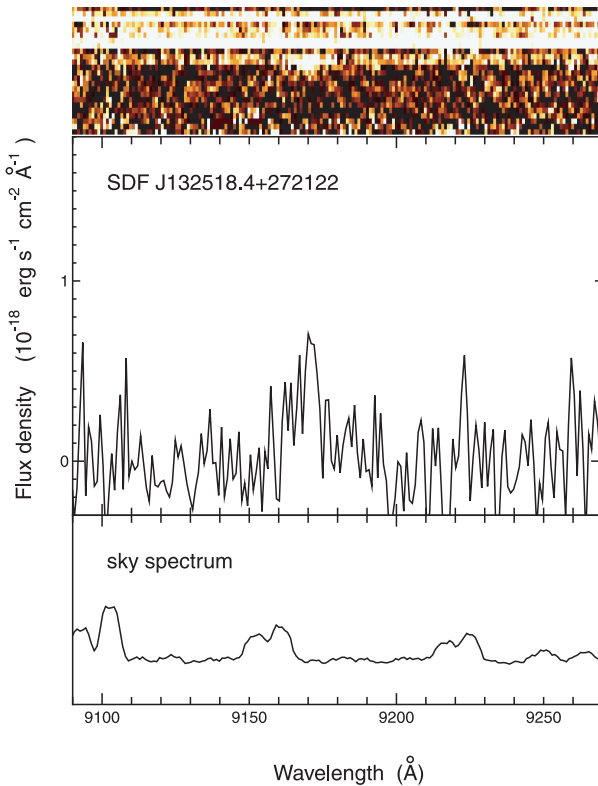

Fig. 8-2. Observed optical spectra of five single-line objects (No. 16 SDF J132518.4 + 272122).
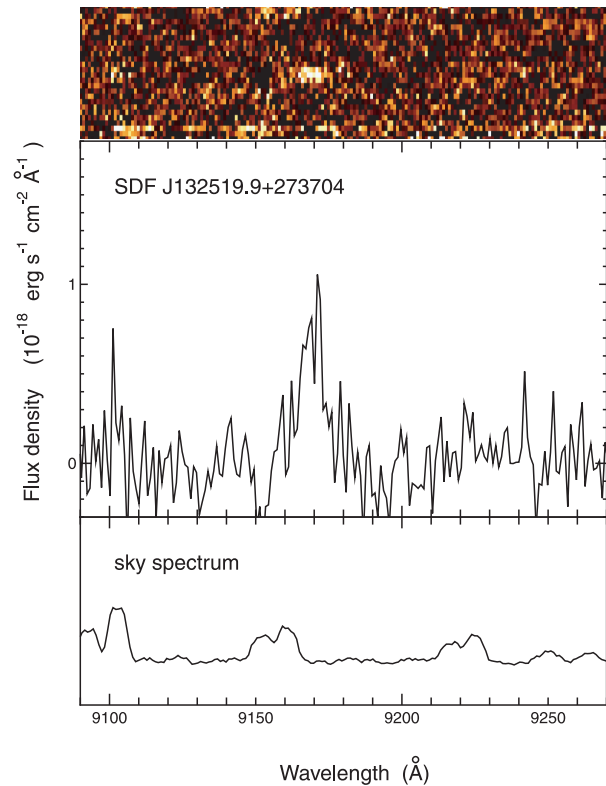

Fig. 8-3. Observed optical spectra of five single-line objects (No. 17 SDF J132519.9 + 273704).
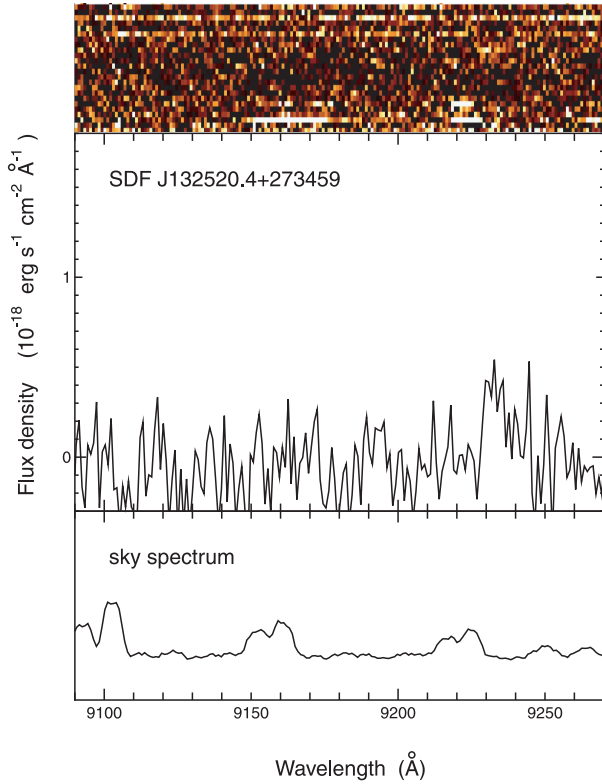
Fig. 8-4. Observed optical spectra of five single-line objects (No. 18 SDF J132520.4 + 273459).
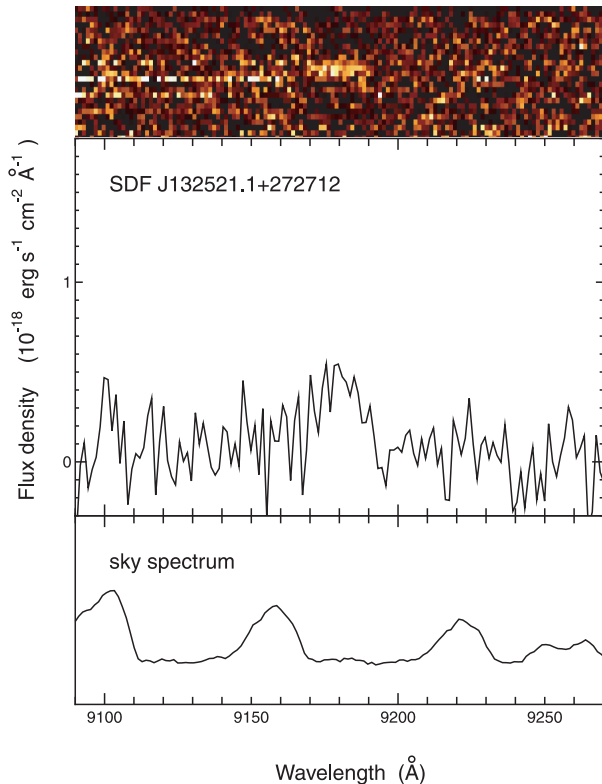

Fig. 8-5. Observed optical spectra of five single-line objects (No. 19 SDF J132521.1 + 272712).
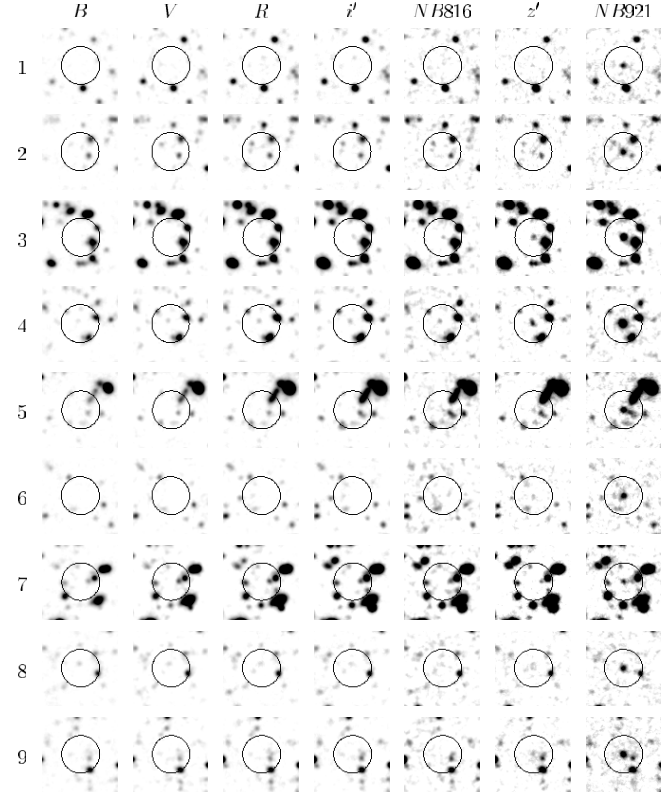

Fig. 9. Thumbnail images of the four LAE candidates. North is up and east is left. The field of view is $16'' \times 16''$, and the diameter of the circle is $8''$.

3.3. Morphological Structures of LAEs

Since our final PSF size is $0.''98$, it seems difficult to investigate the structural properties of the nine LAEs. However, some *NB921* CCD frames were obtained under $0.''5$–$0.''7$ conditions during our observing runs. Using only these data, we made a high-resolution *NB921* image with a PSF of $0.''71$. The integration time for this image was 37215.7 seconds, $\simeq 70\%$ of the total integration time (see table 1).

In figure 10, we show newly made *NB921* images of the nine LAEs. Their azimuthal radial profiles are also shown in figure 11. Their sizes (FWHM) range from $0.''81$ to $1.''02$, as given in table 6. Although we do not conclude that all LAEs are spatially resolved in our *NB921* images, some of them (e.g., Nos. 4 and 8) appear to be spatially extended. After deconvolution with the PSF size, we obtain their sizes between $0.''39$ and $0.''73$, corresponding to $\simeq (2$–$4)\,h_{0.7}^{-1}$ kpc. It is thus suggested that gaseous matter around LAE host galaxies are spatially extended up to several kpc at $z \approx 6.6$ in some cases. Imaging with Advanced Camera for Surveys on board the Hubble Space Telescope with the z(F850LP) filter will be important to investigate their detailed Lyα morphologies.

3.4. Comments on Possible Amplification by Gravitational Lensing

The SDF is a so-called blank field and thus there is no apparent cluster of galaxies known to date at low and

Table 5. Star-formation properties of the nine LAEs.

No.	Name	$f^{\mathrm{spec}}(\mathrm{Ly}\alpha)$ $(10^{-18}\,\mathrm{erg\,s^{-1}\,cm^{-2}})$	$L^{\mathrm{spec}}(\mathrm{Ly}\alpha)$ $(10^{42}\,h_{0.7}^{-2}\,\mathrm{erg\,s^{-1}})$	$SFR^{\mathrm{spec}}(\mathrm{Ly}\alpha)$ $(h_{0.7}^{-2}\,M_\odot\,\mathrm{yr^{-1}})$	FWHM (Å)	FWHM $(\mathrm{km\,s^{-1}})$
1	SDF J132352.7+271622	7.31	3.56	3.24	14.0	458
2	SDF J132353.1+271631	8.22	4.00	3.64	10.6	347
3	SDF J132408.3+271543	16.60	8.13	7.39	7.5	245
4	SDF J132415.7+273058	19.60	9.55	8.69	10.2	334
5	SDF J132418.3+271455	10.95	5.41	4.92	< 9.0	< 293
6	SDF J132418.4+273345	19.43	9.35	8.51	7.8	256
7	SDF J132432.5+271647	6.17	3.05	2.77	9.7	316
8	SDF J132518.8+273043	7.29	3.60	3.28	6.5	212
9	SDF J132522.3+273520	15.48	7.69	7.00	5.5	179
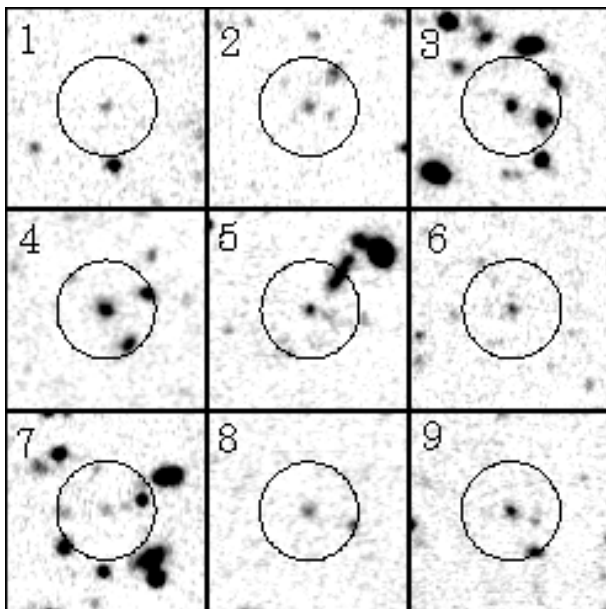
Fig. 10. High-resolution (PSF = 0.″71) *NB921* images of the nine LAEs. The number given in each panel corresponds to that given in tables 2, 4, 5, 6, and 7.
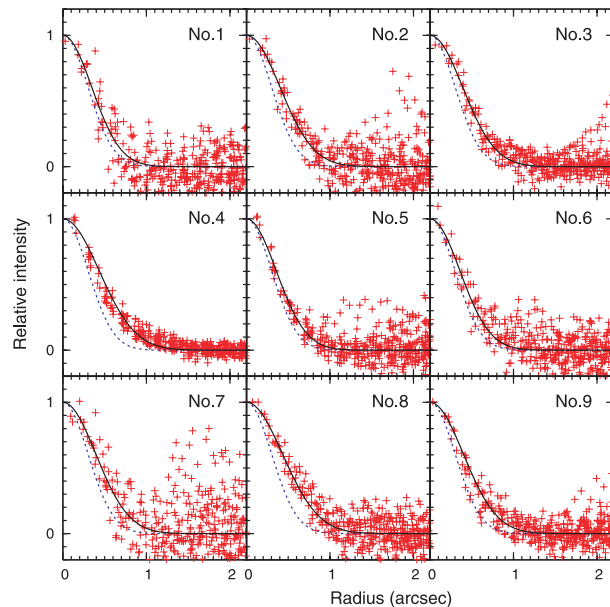
Fig. 11. Surface brightness radial distribution of the nine LAEs. The point-spread function is shown by a dashed blue curve and the best fit profile by black one in each panel. The number given in each panel corresponds to that given in tables 2, 4, 5, 6, and 7.

intermediate redshifts in our field. In this respect, our survey may not suffer from strong amplification by gravitational lensing, unlike several surveys made with the help of gravitational lensing (Ellis et al. 2001; Hu et al. 2002; Santos et al. 2004; Kneib et al. 2004; Pelló et al. 2004a). However, any high-z objects could suffer from gravitational lensing because of a larger optical depth for lensing (Wyithe, Loeb 2002; Shioya et al. 2002). Therefore, it is possible that some LAEs found in our survey could be gravitationally amplified by a foreground galaxy lying close to their lines of sight.

In order to check such possibilities, we examined carefully our i' and z' images for all the nine objects. We also examined our B, V, and R images to check whether or not there are any foreground galaxies. As shown in figures 9 and 10, there are some galaxies that could be foreground galaxies around each LAE. For example, a probable foreground object is found to be located at 0.″8 NW of SDF J132418.3+271455. We listed all

such foreground galaxies within a radius of 4″. We then evaluated the magnification factor for each LAE in the following way (Shioya et al. 2002; see also Yamada et al. 2003): (1) We estimate its photometric redshift and rest-frame B-band luminosity based on our optical broad-band photometric data for each foreground galaxy, if any. (2) We estimated its stellar velocity dispersion using the Tully–Fisher relation and the B-band luminosity estimated above. (3) We estimated the magnification factor based on the singular isothermal sphere model for gravitational lensing. We found that the amplification factor by gravitational lensing is smaller than 1.1 for all the cases. It is also noted that there is no counter image for each LAE within the limiting magnitude, and thus the gravitational amplification factor should be less than a factor of ~ 2, being consistent with the above factor. Therefore, we conclude that our LAE sample did not suffer from strong amplification by the gravitational lensing. This allows us to perform simple

Table 6. Full width at half maximum size of the nine LAEs.

No.	Name	$FWHM$	$FWHM_{\mathrm{cor}}$*	$FWHM_{\mathrm{cor}}$
		('')	('')	$(h_{0.7}^{-1}\,\mathrm{kpc})$
1	SDF J132352.7 + 271622	0.81 ± 0.04	0.39 ± 0.04	2.1 ± 0.2
2	SDF J132353.1 + 271631	0.95 ± 0.03	0.63 ± 0.03	3.5 ± 0.1
3	SDF J132408.3 + 271543	0.92 ± 0.02	0.59 ± 0.02	3.2 ± 0.1
4	SDF J132415.7 + 273058	1.02 ± 0.02	0.73 ± 0.02	4.0 ± 0.1
5	SDF J132418.3 + 271455	0.84 ± 0.02	0.45 ± 0.02	2.5 ± 0.1
6	SDF J132418.4 + 273345	0.84 ± 0.04	0.45 ± 0.04	2.5 ± 0.2
7	SDF J132432.5 + 271647	0.93 ± 0.04	0.60 ± 0.04	3.3 ± 0.2
8	SDF J132518.8 + 273043	1.02 ± 0.03	0.73 ± 0.03	4.0 ± 0.2
9	SDF J132522.3 + 273520	0.94 ± 0.03	0.62 ± 0.03	3.4 ± 0.2

* Deconvolved with a PSF size of 0.''71.

statistical analyses for our sample of LAEs, such as the number density and the star-formation rate density at $z = 6.6$.

4. Discussion

4.1. The Number Density of LAEs at $z \approx 6.6$

First, we estimated the number density of LAEs at $z \simeq 6.6$ and compared it with those at other redshifts. Our sample of LAE candidates consists of 58 objects. Then, our optical spectroscopy found that nine objects are LAEs at $z \simeq 6.5$–6.6 among the 20 objects in our spectroscopic sample. Therefore, from a statistical point of view, $\approx 45\%$ of our photometrically selected candidates are expected to be LAEs at $z \approx 6.6$; note again that the nine galaxies for which optical spectroscopy was made were randomly selected from the photometric sample. The limiting magnitude of our sample, $NB921 = 26.54$, corresponds roughly to $f(\mathrm{Ly}\,\alpha) \simeq 4.1 \times 10^{-18}\,\mathrm{erg\,s^{-1}\,cm^{-2}}$, or $L(\mathrm{Ly}\,\alpha) \simeq 2.0 \times 10^{42}\,h_{0.7}^{-2}\,\mathrm{erg\,s^{-1}}$ for our adopted cosmology. Since the survey volume of our survey is $217200\,h_{0.7}^{-3}\,\mathrm{Mpc^3}$, we obtain the number density of LAEs brighter than this limiting luminosity to be $n(\mathrm{LAE}) \simeq 58 \times 0.45/217200 \simeq 1.2 \times 10^{-4}\,h_{0.7}^{3}\,\mathrm{Mpc^{-3}}$.

It is interesting to compare our result with previous studies on LAEs at high redshift. Note, however, that the detection completeness is not taken into account in later discussion because it is difficult to estimate it for each survey. Ouchi et al. (2003) have made a wide-field survey of LAEs at $z \simeq 4.9$. From their data, we estimate that the number density of LAEs at $z \simeq 4.9$ brighter than $L(\mathrm{Ly}\,\alpha) = 2.4 \times 10^{42}\,h_{0.7}^{-2}\,\mathrm{erg\,s^{-1}}$ is $\simeq 2 \times 10^{-4}\,h_{0.7}^{3}\,\mathrm{Mpc^{-3}}$ (M. Ouchi, private communication), which is close to that for our $z \simeq 6.6$ LAEs. Rhoads and Malhotra (2001) also carried out a similar survey for $z = 5.7$ LAEs; the limiting luminosity of their survey, $\approx 5.3 \times 10^{42}\,h_{0.7}^{-2}\,\mathrm{erg\,s^{-1}}$, is brighter than ours (see also Rhoads et al. 2003). They found in their sample the number density of LAEs to be $\simeq 4 \times 10^{-5}\,h_{0.7}^{3}\,\mathrm{Mpc^{-3}}$. If we limit our $z \simeq 6.6$ LAE sample to Rhoads et al. 's (2003) limiting luminosity, we obtain $\simeq 2 \times 10^{-5}\,h_{0.7}^{3}\,\mathrm{Mpc^{-3}}$. Similarly, we obtain $\simeq 4 \times 10^{-5}\,h_{0.7}^{3}\,\mathrm{Mpc^{-3}}$ for Ouchi et al.'s (2003) sample. These results indicate that the number density of LAEs does not change significantly from $z \simeq 4.9$ to 6.6. Combined with a result given in Ouchi et al.

(2003) that the number density of $z \simeq 4.9$ LAEs is not clearly different from that of $z = 3.4$ LAEs in Cowie and Hu's (1998) sample, we conclude that LAEs do not evolve in number from $z \simeq 3.4$ to 6.6 within the uncertainties in the data.

4.2. The Star-Formation Rate of LAEs at $z \approx 6.6$

4.2.1. The star-formation rate estimated from Ly α luminosity

Next, we estimate the star-formation rate of the LAEs at $z \approx 6.6$. We have two kinds of SFRs: one is based on our optical spectroscopy and the other is based on our continuum-subtracted $NB921$ data.

First, we discuss the SFRs based on our spectroscopy. The observed Ly α flux, Ly α luminosity, and star-formation rate, $SFR(\mathrm{Ly}\,\alpha)$, of each LAE are summarized in table 5. Note that the $SFR(\mathrm{Ly}\,\alpha)$ is estimated by using the relation (Kennicutt 1998; Brocklehurst 1971)

$$SFR(\mathrm{Ly}\,\alpha) = 9.1 \times 10^{-43} L(\mathrm{Ly}\,\alpha)\,M_\odot\,\mathrm{yr^{-1}}, \tag{8}$$

where the Salpeter initial mass function with $(m_{\mathrm{lower}}, m_{\mathrm{upper}}) = (0.1\,M_\odot, 100\,M_\odot)$ is adopted. The SFRs obtained for the nine LAEs range from $\approx 3\,h_{0.7}^{-2}\,M_\odot\,\mathrm{yr^{-1}}$ to $\approx 9\,h_{0.7}^{-2}\,M_\odot\,\mathrm{yr^{-1}}$ with an average of $5.7 \pm 2.3\,h_{0.7}^{-2}\,M_\odot\,\mathrm{yr^{-1}}$. These values are comparable to those of LAEs at $z \simeq 5.1$–5.8 (e.g., Taniguchi et al. 2003b and references therein). The total spectroscopic SFR for the nine LAEs amounts to

$$SFR^{\mathrm{spec}}(\mathrm{Ly}\,\alpha) \simeq 49.4\,h_{0.7}^{-2}\,M_\odot\,\mathrm{yr^{-1}}. \tag{9}$$

It should be mentioned that the SFRs estimated above are lower limits because it is quite likely that a blue half or more of the Ly α emission may be absorbed by dust grains in the galaxy, itself, and by the intergalactic H I gas (e.g., Hu et al. 2002; Haiman 2002). Therefore, it would be desirable to study the rest-frame UV-optical continuum (Hu et al. 2002; Kodaira et al. 2003).

Second, we discuss SFRs based on the continuum-subtracted $NB921$ data; $SFR^{\mathrm{image}}(\mathrm{Ly}\,\alpha)$. Our results are summarized in table 7; note that we give the photometric SFRs for all 58 LAE candidates. The frequency distributions of Ly α luminosity for all 58 LAE candidates are shown in figure 12. The Ly α luminosity of the two sources, SDF J132353.1 + 271631 (No. 2) and SDF J132518.8 + 273043, is given as an upper-limit. This is due to the fact that the bandpass-corrected z'

Table 7. Star-formation properties of our LAE candidates.

No.	Name	$L^{\mathrm{image}}(\mathrm{Ly}\alpha)^*$	$L_\nu(\mathrm{UV})$	$SFR^{\mathrm{image}}(\mathrm{Ly}\alpha)$	$SFR(\mathrm{UV})$
		$(10^{42}\,\mathrm{erg\,s^{-1}})$	$(10^{29}\,\mathrm{erg\,s^{-1}\,Hz^{-1}})$	$(M_\odot\,\mathrm{yr^{-1}})$	$(M_\odot\,\mathrm{yr^{-1}})$
1	SDF J132352.7+271622	4.4	< 6.4	4.0	< 9.0
2	SDF J132353.1+271631	4.6	13.9	4.2	19.4
3	SDF J132408.3+271543	9.2	25.0	8.4	35.0
4	SDF J132415.7+273058	13.7	30.1	12.4	42.2
5	SDF J132418.3+271455	9.4	< 6.4	8.6	< 9.0
6	SDF J132418.4+273345	6.6	< 6.4	6.0	< 9.0
7	SDF J132432.5+271647	4.8	< 6.4	4.4	< 9.0
8	SDF J132518.8+273043	4.4	11.2	4.0	15.6
9	SDF J132522.3+273520	7.1	13.9	6.5	19.5
10	SDF J132406.5+271634	3.4	13.9	3.1	19.4
11	SDF J132410.8+271928	4.3	21.0	3.9	29.4
12	SDF J132417.9+271746	5.4	< 6.4	4.9	< 9.0
13	SDF J132428.7+273049	4.6	< 6.4	4.2	< 9.0
14	SDF J132500.9+272030	4.1	< 6.4	3.7	< 9.0
15	SDF J132515.5+273714	5.5	< 6.4	5.0	< 9.0
16	SDF J132518.4+272122	15.4	8.4	14.0	11.7
17	SDF J132519.9+273704	5.1	< 6.4	4.7	< 9.0
18	SDF J132520.4+273459	4.0	10.5	3.7	14.6
19	SDF J132521.1+272712	5.1	12.9	4.6	18.1
20	SDF J132525.3+271932	2.4	14.6	2.2	20.4
21	SDF J132338.4+274652	4.5	< 6.4	4.1	< 9.0
22	SDF J132338.6+272940	4.1	< 6.4	3.8	< 9.0
23	SDF J132342.2+272644	5.4	< 6.4	4.9	< 9.0
24	SDF J132343.2+272452	10.9	7.5	9.9	10.4
25	SDF J132347.7+272360	4.5	< 6.4	4.1	< 9.0
26	SDF J132348.9+271530	5.0	< 6.4	4.5	< 9.0
27	SDF J132349.2+273211	3.6	< 6.4	3.3	< 9.0
28	SDF J132349.2+274546	6.9	< 6.4	6.3	< 9.0
29	SDF J132353.4+272602	6.7	11.3	6.1	15.9
30	SDF J132357.1+272448	3.3	8.0	3.0	11.2
31	SDF J132401.5+273837	3.6	< 6.4	3.3	< 9.0
32	SDF J132402.6+274653	3.2	13.9	2.9	19.5
33	SDF J132410.5+272811	4.0	< 6.4	3.7	< 9.0
34	SDF J132419.3+274125	5.8	< 6.4	5.3	< 9.0
35	SDF J132422.6+274459	5.2	9.2	4.7	12.9
36	SDF J132424.2+272649	2.6	8.8	2.4	12.3
37	SDF J132425.4+272410	3.2	< 6.4	2.9	< 9.0
38	SDF J132425.9+274324	4.4	< 6.4	4.0	< 9.0
39	SDF J132425.0+273606	4.7	< 6.4	4.3	< 9.0
40	SDF J132434.3+274056	5.1	< 6.4	4.6	< 9.0
41	SDF J132435.0+273957	5.4	< 6.4	5.0	< 9.0
42	SDF J132436.6+272223	3.7	< 6.4	3.3	< 9.0
43	SDF J132440.2+272553	4.6	< 6.4	4.1	< 9.0
44	SDF J132443.4+272633	4.2	10.4	3.9	14.5
45	SDF J132444.4+273942	4.8	< 6.4	4.4	< 9.0
46	SDF J132445.6+273033	5.6	8.1	5.1	11.3
47	SDF J132447.7+271106	4.3	9.9	3.9	13.8
48	SDF J132449.5+274237	2.7	< 6.4	2.5	< 9.0
49	SDF J132450.7+272160	4.6	< 6.4	4.2	< 9.0
50	SDF J132455.4+271314	4.0	< 6.4	3.7	< 9.0
51	SDF J132455.8+274015	3.2	< 6.4	2.9	< 9.0
52	SDF J132458.5+273913	10.4	< 6.4	9.5	< 9.0
53	SDF J132458.0+272349	4.4	< 6.4	4.0	< 9.0

Table 7.   (Continued.)

No.	Name	$L^{\mathrm{image}}(\mathrm{Ly}\,\alpha)^*$ $(10^{42}\,\mathrm{erg\,s^{-1}})$	$L_\nu(\mathrm{UV})$ $(10^{29}\,\mathrm{erg\,s^{-1}\,Hz^{-1}})$	$SFR^{\mathrm{image}}(\mathrm{Ly}\,\alpha)$ $(M_\odot\,\mathrm{yr^{-1}})$	$SFR(\mathrm{UV})$ $(M_\odot\,\mathrm{yr^{-1}})$
54	SDF J132503.4+273838	3.3	< 6.4	3.0	< 9.0
55	SDF J132506.4+274047	3.1	< 6.4	2.8	< 9.0
56	SDF J132516.7+272236	5.5	< 6.4	5.0	< 9.0
57	SDF J132528.0+271328	3.9	< 6.4	3.5	< 9.0
58	SDF J132533.4+271420	5.4	< 6.4	4.9	< 9.0

* The UV luminosity at $\lambda = 1260\,\text{Å}$.
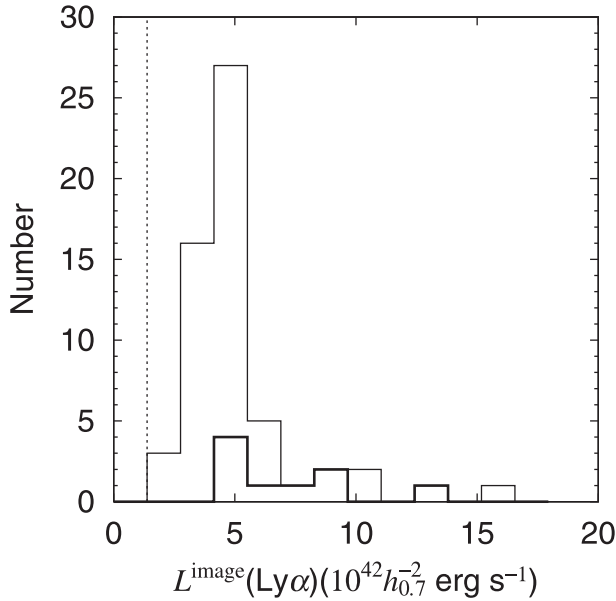
Fig. 12. Histograms of $L^{\mathrm{image}}(\mathrm{Ly}\,\alpha)$ for the photometric sample (58 LAE candidates) and for the nine LAEs. The latter is shown by the thick line. The bins correspond to 1σ ($= 1.4 \times 10^{42}\,h_{0.7}^{-2}\,\mathrm{erg\,s^{-1}}$), 2σ, 3σ, and 4σ, of $L^{\mathrm{image}}(\mathrm{Ly}\,\alpha)$; see table 7 in more details.

Fig. 13. Comparisons between $f^{\mathrm{spec}}(\mathrm{Ly}\,\alpha)$ and $f^{\mathrm{image}}(\mathrm{Ly}\,\alpha)$ for the nine LAEs.

flux (f_{9500}; see table 2) is estimated to be a bit higher because of low signal-to-noise ratios. Although these two upper limit data are present, the SFRs of the nine LAEs confirmed by our spectroscopy range between 3 and $10\,h_{0.7}^{-2}\,M_\odot\,\mathrm{yr^{-1}}$, being similar to that obtained in our spectroscopy. The total photometric SFR for the nine LAEs is estimated to be

$$SFR^{\mathrm{image}}(\mathrm{Ly}\,\alpha) \simeq 58.5\,h_{0.7}^{-2}\,M_\odot\,\mathrm{yr^{-1}}, \qquad (10)$$

being nearly the same as that obtained by the spectroscopy. In figure 13, we compare the observed fluxes of Ly α emission obtained from spectroscopy and imaging for the nine LAEs.

4.2.2. The star formation rate estimated from UV luminosity

We now estimate another SFR derived from the UV continuum luminosity for our sample. The observed z' magnitude can be converted to a UV continuum luminosity at $\lambda = 1260\,\text{Å}$. Using the relation (Kennicutt 1998; see also Madau et al. 1998),

$$SFR(\mathrm{UV}) = 1.4 \times 10^{-28} L_\nu(\mathrm{UV})\,M_\odot\,\mathrm{yr^{-1}} \qquad (11)$$

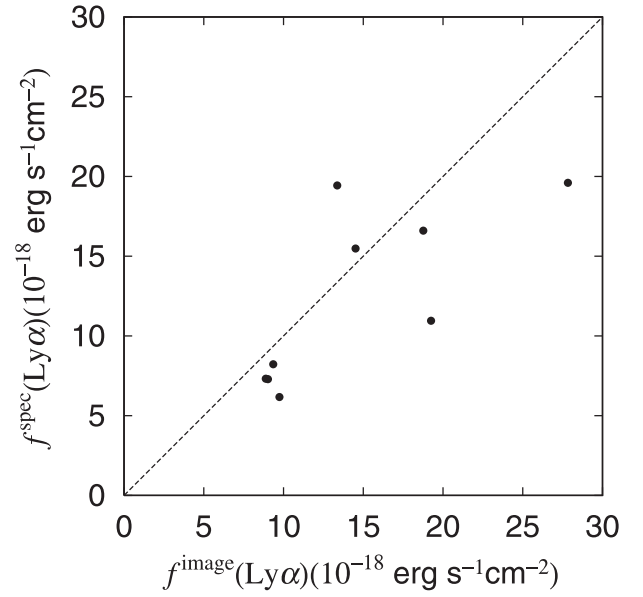where $L_\nu(\mathrm{UV})$ is the UV continuum luminosity in units of

$\mathrm{erg\,s^{-1}\,Hz^{-1}}$, we estimate the SFR based on the rest-frame UV ($\lambda = 1260\,\text{Å}$) continuum luminosity for each object. The results are summarized in table 7. Note that the same initial mass function for $SFR(\mathrm{Ly}\,\alpha)$ was adopted in this estimate. The frequency distributions of UV continuum luminosity for all 58 LAE candidates are shown in figure 14.

4.2.3. Comparisons between SFR(Ly α) and SFR(UV)

We then compared the SFRs derived from the Ly α and the UV photometric data. The result is shown in figure 15; also see table 7. As expected from previous studies (e.g., Hu et al. 2003; Kodaira et al. 2003; Ajiki et al. 2003), we find that $SFR(\mathrm{UV})$ tends to be higher by a factor of 5, on average, than $SFR^{\mathrm{image}}(\mathrm{Ly}\,\alpha)$. The obtained factor seems to be higher than the previous results; e.g., by a factor of 2.

4.3. The Star Formation Rate Density of LAEs at z ≈ 6.6

We now discuss the star-formation history beyond redshift 6 based on our data. We can estimate the total star-formation rate of 58 LAEs in our photometric sample using the equivalent width of the *NB921* flux; $SFR^{\mathrm{image}}(\mathrm{total}) \simeq 276\,h_{0.7}^{-2}\,M_\odot\,\mathrm{yr^{-1}}$. Given the survey volume, $217200\,h_{0.7}^{-3}\,\mathrm{Mpc^3}$, we nominally

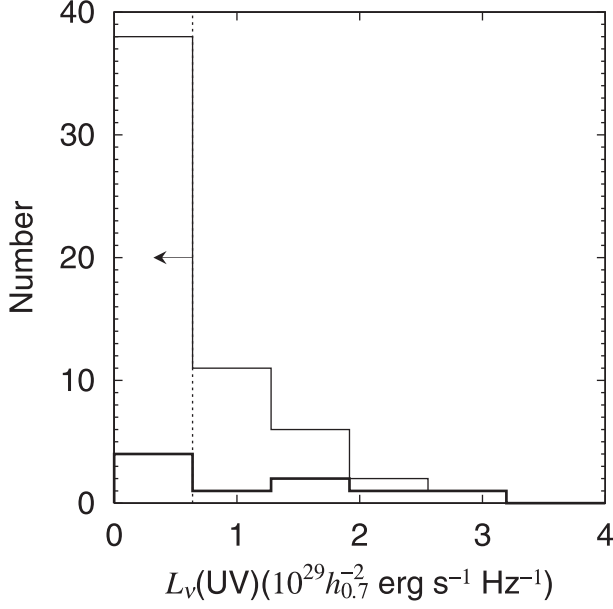**Fig. 14.** Histograms of L_ν(UV) at $\lambda = 1260$ Å for the photometric sample (the 58 LAE candidates) and for the nine LAEs. The latter is shown by the thick line. The bins correspond to $1\,\sigma$ $(= 0.64 \times 10^{29}\, h_{0.7}^{-2}\, \mathrm{erg\,s^{-1}\,Å^{-1}})$, $2\,\sigma$, and $3\,\sigma$ of L_ν(UV); see table 7 in more details.
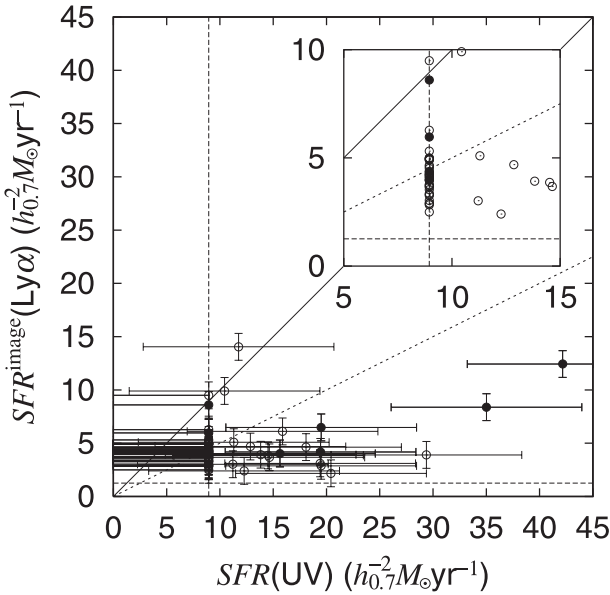
Fig. 15. Comparisons between SFR^{image}(Lyα) and SFR(UV) for the 58 LAE candidates. The nine LAEs are shown by filled circles. The inset shows a close up to see crowded data points for SFR^{image}(Lyα) $h_{0.7}^{-2}\, M_\odot\, \mathrm{yr^{-1}}$ and for SFR(UV) = 5–$15\, h_{0.7}^{-2}\, M_\odot\, \mathrm{yr^{-1}}$.

obtain a star-formation rate density (SFRD) of $\rho_{\mathrm{SFR,upper}} \simeq 1.3 \times 10^{-3}\, h_{0.7}\, M_\odot\, \mathrm{yr^{-1}\, Mpc^{-3}}$. However, this value should be regarded being as an upper bound obtained from our study. Since we estimated the fraction of LAEs in our photometric sample, $f(\mathrm{LAE}) \simeq 0.45$, it seems reasonable to assume that 45% of the LAE candidates are at $z \approx 6.6$.
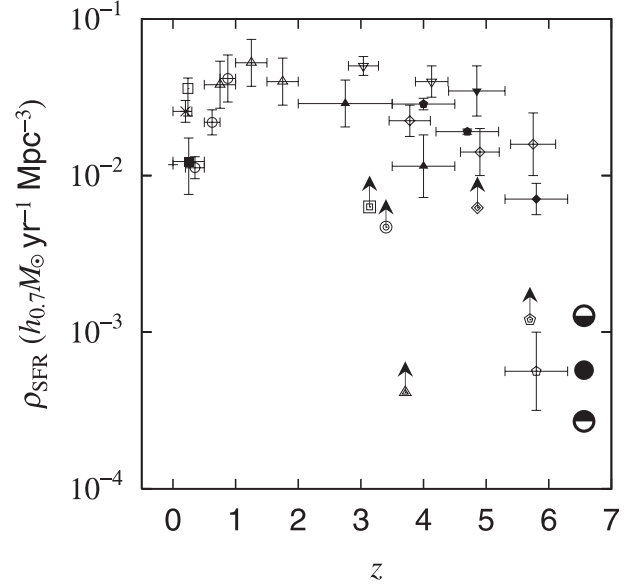

Fig. 16. Star-formation rate density shown as a function of the redshift. Our data points are shown with big symbols; $\rho_{SFR} = 5.5 \times 10^{-4}\, h_{0.7}\, M_\odot\, \mathrm{yr^{-1}\, Mpc^{-3}}$ is shown by the filled circle. $\rho_{SFR}^{\mathrm{upper}}$ is shown by an upper half-filled circle while $\rho_{SFR}^{\mathrm{lower}}$ by an upper half-filled one. The other data sources are Gallego et al. (1995 — plus), Tresse and Maddox (1998 — star), Fujita et al. (2003b — open square), Treyer et al. (1998 — filled square), Lilly et al. (1996 — open circles), Connolly et al. (1997 — open triangles), Madau et al. (1996 — filled triangles), Steidel et al. (1999 — open inverse triangles), Iwata et al. (2003 — filled inverse triangle), Giavalisco et al. (2004b — open diamonds), Bouwens et al. (2004 — filled diamond), Stanway et al. (2004b — open hexagon), and Ouchi et al. (2004 — filled hexagons). For reference, we also show the results of previous Lyα searches at $z \sim 3$–6 by Kudritzki et al. (2000 — double square), Cowie and Hu (1998 — double circle), Fujita et al. (2003a — double triangle), Ouchi et al. (2003 — double diamond), and Ajiki et al. (2003 — double hexagon).

We then obtained the corrected total SFR, $SFR^{\mathrm{image,cor}}$(total) $\simeq 276 \times 0.45 \simeq 124\, h_{0.7}^{-2}\, M_\odot\, \mathrm{yr^{-1}}$. This gives $\rho_{SFR} \simeq 5.7 \times 10^{-4}\, h_{0.7}\, M_\odot\, \mathrm{yr^{-1}\, Mpc^{-3}}$, being consistent with our previous study (Kodaira et al. 2003). Recently, Kurk et al. (2004) made a grism survey for LAEs at $z \approx 6.4$–6.6 and then identified a LAE at $z = 6.518$. Their new type of survey also gave a similar value of SFRD: $\rho_{SFR} \simeq 5.0 \times 10^{-4}\, h_{0.7}\, M_\odot\, \mathrm{yr^{-1}\, Mpc^{-3}}$.

We were also able to obtain a lower bound of the total SFR using the observed Lyα fluxes obtained with our spectroscopy. Using the data given in table 5, we obtained SFR^{spec}(total) $\simeq 49.4\, h_{0.7}^{-2}\, M_\odot\, \mathrm{yr^{-1}}$. This gives a lower bound of SFRD, $\rho_{\mathrm{SFR,lower}} \simeq 2.3 \times 10^{-4}\, h_{0.7}\, M_\odot\, \mathrm{yr^{-1}\, Mpc^{-3}}$.

It is interesting to compare this value with previous estimates between $z = 0$ and $z \sim 6$. In figure 16, we compare this star-formation rate density with those of previous studies compiled by Ajiki et al. (2003) under the same cosmological parameters as those adopted in this paper. In addition, we also show the results obtained from LAE surveys by Cowie and Hu (1998), Kudritzki et al. (2000), Ouchi et al. (2003), and Ajiki et al. (2003) and from LBG surveys by Giavalisco et al. (2004b) and Dickinson et al. (2004).

Our SFRD together with those based on the LAE surveys tend to give smaller values with respect to those obtained from LBG ones at $z \sim 3$–6. It should be reminded here again that we applied neither any reddening correction nor integration by assuming a certain luminosity function for the LAEs. Previous studies have shown that the SFR based on the Lyα luminosity is smaller by a factor of two or more than that based on the UV continuum (Hu et al. 2002; Kodaira et al. 2003). Kodaira et al. (2003) also showed that the SFR based on the rest-frame optical continuum gives a value several times as high as that based on the Lyα luminosity. More recently, Reddy and Steidel (2004) have shown from an analysis of GOODS multiwavelength data (see for GOODS, Giavalisco et al. 2004a) that the SFR based on X-ray data is higher by a factor of 5 than that based on the UV luminosity. In addition, integration using a luminosity function of LAEs also increases the SFR by a factor of two or more (see Ajiki et al. 2003). Although we do not still have a well-defined Lyα luminosity function based on a large sample of LAEs (e.g., Santos et al. 2004; Hu et al. 2004), the SFR derived here for our sample of LAEs at $z \approx 6.6$ may be smaller by a factor of several than the real value; i.e., ρ_{SFR} is on the order of $10^{-2} h_{0.7}^{-2} M_\odot \, \mathrm{yr}^{-1} \, \mathrm{Mpc}^{-3}$, or higher.

Finally, we comment on SFRDs based on so-called i'-dropout samples. In addition to the follow-up optical spectroscopy of LAE candidates at $z \approx 6.6$ (this work), we also conducted optical spectroscopy of a sample of i'-dropouts found in the SDF (details will be given elsewhere). During this follow-up spectroscopy, we found a LAE at $z = 6.33$ (Nagao et al. 2004). Its z'-band flux is dominated by strong Lyα emission, rather than the stellar UV continuum. If such strong LAEs could be involved in a photometric sample of i'-dropouts, we would overestimate SFRD. This issue shall be addressed in our forthcoming papers.

References

Ajiki, M., et al. 2002, ApJ, 576, L25

Ajiki, M., et al. 2003, AJ, 126, 2091

Bertin, E., & Arnouts, S. 1996, A&AS, 117, 393

Bouwens, R. J., et al. 2004, ApJ, 606, L25

Brocklehurst, M. 1971, MNRAS, 153, 471

Bruzual, G., & Charlot, S. 2003, MNRAS, 344, 1000

Connolly, A. J., Szalay, A. S., Dickinson, M., Subbarao, M. U., & Brunner, R. J. 1997, ApJ, 486, L11

Cowie, L. L., & Hu, E. M. 1998, AJ, 115, 1319

Dawson, S., Stern, D., Bunker, A. J., Spinrad, H., & Dey, A. 2001, AJ, 122, 598

Dickinson, M., et al. 2004, ApJ, 600, L99

Ellis, R., Santos, M. R., Kneib, J.-P., & Kuijken, K. 2001, ApJ, 560, L119

Fioc, M., & Rocca-Volmerange, B. 1997, A&A, 326, 950

Fujita, S. S., et al. 2003a, AJ, 125, 13

Fujita, S. S., et al. 2003b, ApJ, 586, L115

Gallego, J., Zamorano, J., Aragón-Salamanca, A., & Rego, M. 1995, ApJ, 455, L1; Errata 1996, 459, L43

Giavalisco, M., et al. 2004a, ApJ, 600, L93

Giavalisco, M., et al. 2004b, ApJ, 600, L103

Haiman, Z. 2002, ApJ, 576, L1

Hu, E. M., Cowie, L. L., Capak, P., McMahon, R. G., Hayashino, T., & Komiyama, Y. 2004, AJ, 127, 563

Hu, E. M., Cowie, L. L., McMahon, R. G., Capak, P., Iwamuro, F., Kneib, J.-P., Maihara, T., & Motohara, K. 2002, ApJ, 568, L75; Erratum, 576, L99

Iwata, I., Ohta, K., Tamura, N., Ando, M., Wada, S., Watanabe, C., Akiyama, M., & Aoki, K. 2003, PASJ, 55, 415

Iye, M., et al. 2004, PASJ, 56, 381

Kaifu, N., et al. 2000, PASJ, 52, 1

Kashikawa, N., et al. 2002, PASJ, 54, 819

Kashikawa, N., et al. 2003, AJ, 125, 53

Kashikawa, N., et al. 2004, PASJ, 56, 1011

Kennicutt, R. C., Jr. 1998, ARA&A, 36, 189

Kneib, J.-P., Ellis, R. S., Santos, M. R., & Richard, J. 2004, ApJ, 607, 697

Kodaira, K., et al. 2003, PASJ, 55, L17

Kudritzki, R.-P., et al. 2000, ApJ, 536, 19

Kurk, J. D., Cimatti, A., di Serego Alighieri, S., Vernet, J., Daddi, E., Ferrara, A., & Ciardi, B. 2004, A&A, 422, L13

Lilly, S. J., Le Fevre, O., Hammer, F., & Crampton, D. 1996, ApJ, 460, L1

Madau, P., Ferguson, H. C., Dickinson, M. E., Giavalisco, M., Steidel, C. C., & Fruchter, A. 1996, MNRAS, 283, 1388

Madau, P., Pozzetti, L., & Dickinson, M. 1998, ApJ, 498, 106

Maier, C., et al. 2003, A&A, 402, 79

Maihara, T., et al. 2001, PASJ, 53, 25

Miyazaki, S., et al. 2002, PASJ, 54, 833

Nagao, T., et al. 2004, ApJ, 613, L9

Ostriker, J. P., & Gnedin, N. Y. 1996, ApJ, 472, L63

Ouchi, M., et al. 2001, BAAS, 33, 1313

Ouchi, M., et al. 2003, ApJ, 582, 60

Ouchi, M., et al. 2004a, ApJ, 611, 660

Ouchi, M., et al. 2004b, ApJ, 611, 685

Pelló, R., Richard, J., Le Borgne, J.-F., & Schaerer, D. 2004b, astro-ph/0407194

Pelló, R., Schaerer, D., Richard, J., Le Borgne, J.-F., & Kneib, J.-P. 2004a, A&A, 416, L35

Reddy, N. A., & Steidel, C. C. 2004, ApJ, 603, L13

Rhoads, J. E., et al. 2003, AJ, 125, 1006

Rhoads, J. E., et al. 2004, ApJ, 611, 59

Rhoads, J. E., & Malhotra, S. 2001, ApJ, 563, L5

Santos, M. R., Ellis, R. S., Kneib, J.-P., Richard, J., & Kuijken, K. 2004, ApJ, 606, 683

Shimasaku, K., et al. 2003, ApJ, 586, L111

Shimasaku, K., et al. 2004, ApJ, 605, L93

Shioya, Y., et al. 2002, PASJ, 54, 975

Spinrad, H. 2005 Astrophysics Update   in press (astro-ph/0308411)

Stanway, E. R., et al. 2004a, ApJ, 604, L13

Stanway, E. R., McMahon, R. G., & Bunker, A. 2004b, MNRAS submitted (astro-ph/0403585)

Steidel, C. C., Adelberger, K. L., Giavalisco, M., Dickinson, M., & Pettini, M. 1999, ApJ, 519, 1

Steidel, C. C., Giavalisco, M., Pettini, M., Dickinson, M., & Adelberger, K. L. 1996, ApJ, 462, L17

Stern, D., et al. 2004, ApJ   submitted (astro-ph/0407409)

Stern, D., Bunker, A., Spinrad, H., & Dey, A. 2000, ApJ, 537, 73

Taniguchi, Y. 2005, in Proc. Multiwavelength Mapping of Galaxy Formation and Evolution   in press (astro-ph/0312228)

Taniguchi, Y., et al. 2003a, ApJ, 585, L97

Taniguchi, Y., Shioya, Y., Ajiki, M., Fujita, S. S., Nagao, T., & Murayama, T. 2003b, J. Korean Asrtron. Soc., 36, 123 (astro-ph/0306409); Erratum, 36, 283

Totani, T., Yoshii, Y., Iwamuro, F., Maihara, T., & Motohara, K. 2001a, ApJ, 550, L137

Totani, T., Yoshii, Y., Iwamuro, F., Maihara, T., & Motohara, K. 2001b, ApJ, 558, L87

Totani, T., Yoshii, Y., Maihara, T., Iwamuro, F., & Motohara, K. 2001c, ApJ, 559, 592

Tresse, L., & Maddox, S. J. 1998, ApJ, 495, 691

Treyer, M. A., Ellis, R. S., Milliard, B., Donas, J., & Bridges, T. J. 1998, MNRAS, 300, 303

Weatherley, S. J., Warren, S. J., & Babbedge, T. S. R. 2004, A&A, 428, L29

Wyithe, J. S. B., & Loeb, A. 2002, ApJ, 577, 57

Yagi, M., Kashikawa, N., Sekiguchi, M., Doi, M., Yasuda, N., Shimasaku, K., & Okamura, S. 2002, AJ, 123, 66

Yamada, S. F., et al. 2003, PASJ, 55, 733